NUREG/CR-6824
ANL-02/37

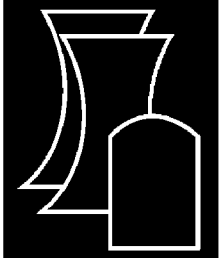

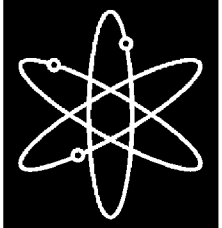

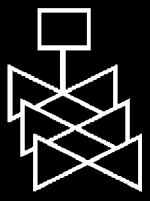

Materials Behavior in HTGR Environments

Argonne National Laboratory

U.S. Nuclear Regulatory Commission
Office of Nuclear Regulatory Research
Washington, DC 20555-0001

NUREG/CR-6824
ANL-02/37

Materials Behavior in HTGR Environments

Manuscript Completed: February 2003
Date Published: July 2003

Prepared by
K. Natesan, A. Purohit, S. W. Tam

Argonne National Laboratory
9700 South Cass Avenue
Argonne, IL 60439

C. A. Greene, NRC Project Manager

Prepared for
Division of Engineering Technology
Office of Nuclear Regulatory Research
U.S. Nuclear Regulatory Commission
Washington, DC 20555-0001
NRC Job Code Y6537

Materials Behavior in HTGR Environments

by

K. Natesan, A. Purohit, and S. W. Tam

Abstract

The report reviews and evaluates data currently available on materials performance and long-term behavior in High-Temperature Gas-Cooled Reactors (HTGRs), including the Gas Turbine-Modular Helium Reactor (GT-MHR) and the Pebble Bed Modular Reactor (PBMR). As part of the evaluation, the report identifies the materials that have been used in HTGRs, their functions, and the environmental conditions under which they need to perform adequately. The report identifies the materials used for structural applications (such as pressure vessel and reactor primary circuit components, including internals) and for the power conversion system, with emphasis on gas-turbine-based HTGRs. The report examines the chemistry of the primary-circuit helium environment from the standpoint of type and concentration of impurities. A framework is presented for analyzing gas-solid interactions in single and bioxidant conditions, and the data on materials scaling behavior are compared from several research programs. This report discusses the available data on the mechanical properties (such as creep, fatigue, creep fatigue, and crack growth) of candidate materials in a helium environment. Available information on the carburization, decarburization, oxidation, and aging of structural materials and their effects on mechanical properties is summarized. From the materials standpoint, the report also discusses the role of particulate-laden gases in corrosion-erosion and the possible effects on materials from off-normal situations in the operation of the reactors. The report makes several recommendations to supplement the data on environmental effects on materials, on mechanical properties of structural and power conversion materials, and on alternative candidate alloys for application in HTGRs.

Contents

Figures

Tables

Executive Summary

The High Temperature Gas Reactor (HTGR) concept currently considered by the Member States of the IAEA's International Working Group on Gas Cooled Reactors (IWGGCR) involves helium as the coolant and a closed-cycle gas turbine for power generation with a core outlet/gas turbine inlet temperature of 850°C and a net plant efficiency of 47%. In these designs, the helium from the core is used directly to drive the turbines or indirectly to heat the air or nitrogen, which drives the turbines. The system concepts include the Gas Turbine-Modular Helium Reactor (GT-MHR) developed by a consortium led by General Atomics in the U.S., the Pebble Bed Modular Reactor (PBMR) designed by ESKOM of South Africa and British Nuclear Fuels of U.K., and the High Temperature Engineering Test Reactor (HTTR) of Japan.

The objective of this report is to review and evaluate the available information on performance and on long-term behavior of materials in environments that are typical of high-temperature helium-cooled reactors. As a part of this evaluation, the materials that have been used in HTGRs, their functions, and the environmental conditions under which they have operated are identified. The materials to be used in new HTGRs, the functions they will serve, and the anticipated environmental conditions under which they are expected to operate are likewise identified. Those HTGR conditions that may affect material property response, such as the steady-state operating environment, component geometry, and off-normal conditions, are discussed and evaluated.

The primary helium coolant in the gas-turbine-based HTGRs is expected to be at temperatures in the range of 850-900°C, and the selected materials should have adequate performance over long service life at temperatures in the range of 900-950°C. There are several issues in materials selection for such an application, and reliable component performance requires a significant technical database for the selection of materials and for assessment of the long-term effects on the materials behavior in the service environment. This report reviews the literature on HTGR materials properties and environmental effects on the behavior of metallic materials. The key technical issues addressed in this report are:

- Baseline mechanical property data,
- Effects of helium coolant chemistry on materials degradation,
- Corrosion effects on mechanical properties of candidate materials,
- Fission product release and its effect on materials,
- Corrosion-erosion due to particulate-laden gas flow.

Section 2 of the report discusses the baseline mechanical property data for several candidate materials that are being considered for application in HTGRs. The properties include tensile strength, creep rupture, low-cycle fatigue, creep fatigue, and fracture toughness. The information is used to assess the adequacy and applicability of data for the design and service life of components in HTGR environments. The availability and adequacy of design codes, rules, and procedures for various components are discussed in a companion report.

Among the materials, 2 1/4Cr-1Mo and modified 9Cr-1Mo ferritic steels are considered for application in reactor pressure vessels. Fe-Cr-Ni alloys such as Alloy 800H and austenitic stainless steels are considered for recuperators and reactor internals. Alloys such as 617,

Hastelloy X, and Hastelloy XR are considered for components that will be exposed to helium coolant at temperatures up to 900°C. Alloys such as 713LC and Mo-TZM are considered for the turbine blade. Alloys such as A286, 706, and 718, are examined for turbine disk application.

Section 3 examines the influence of helium coolant on the chemical compatibility of structural materials that are planned for use in HTGRs. Helium, because of its chemical inertness and attractive thermal properties, is used as a primary coolant in HTGRs. However, the primary coolant in an operating HTGR is expected to be contaminated by small amounts of gaseous impurities such as H_2, H_2O, CH_4, CO, CO_2, and O_2 from a variety of sources in the reactor circuit.

Several conclusions can be drawn from this evaluation:

- Most materials research and development programs, in support of HTGRs, were conducted in the 1960s to early 1980s. The thrust of these programs was to develop a database on materials for application in steam-cycle and process-nuclear-heat based HTGRs.

- Very little work was done during this period on materials with emphasis on direct and/or indirect gas-turbine-based HTGRs.

- The primary materials for high temperature application in HTGRs that have been studied in detail are Alloys 800H and 617 and Hastelloy X. Among them, Alloy 800H is code certified for temperatures up to 760°C for use in nuclear systems. A draft code case for Alloy 617 has been developed. A substantial database has been developed for both Alloys 800H and 617, and a limited database exists for Hastelloy X. Since the high temperature scaling in Hastelloy X has not been adequate, a modified version, Hastelloy XR, has been developed in programs conducted in Japan.

- Even though helium, by itself, is inert towards the materials, it is often contaminated by small amounts of gaseous impurities such as H_2, H_2O, CH_4, CO, CO_2, and O_2 from a variety of sources in the reactor circuit. The gas chemistry and the thermodynamic activity for carbon and oxygen in the gas phase are difficult to ascertain because of the nonequilibrium nature of the gas mixture. Furthermore, most studies on gas chemistry simulations were performed close to atmospheric pressure, whereas the system pressure in the reactor is ≈7 MPa.

- Structural alloys can be significantly corroded by the gaseous impurities in helium at elevated temperatures. Past studies have shown that the corrosion of heat resistant materials such as austenitic stainless steels, Alloy 800H, and Alloy 617 may involve oxidation, carburization, and decarburization depending on the exposure temperature, carbon activity in the gas phase, and the alloy composition. Furthermore, the corrosion process is “dynamic” in that it is dictated by the exposure time, gas chemistry variations, integrity of the corrosion product scales, and presence of particulates in the gas phase. A thermodynamic framework that includes evaluation of chemistry under nonequilibrium conditions is presented in this report. The available corrosion information for several candidate alloys exposed to helium

environments, is evaluated to address the scaling behavior and its relationship to gas chemistry.

- Available data are reviewed on the mechanical properties of candidate alloys in a helium environment with low levels of impurities. In most of these tests the environment contained sufficiently high H_2O (typical of steam-cycle-based HTGRs), and the alloys predominantly developed oxide scales on the surface during mechanical testing. The mechanical properties evaluated included creep, creep rupture, low- and high-cycle fatigue, creep fatigue, and fracture toughness.

- In studies that were conducted in a helium environment with reduced levels of H_2O, Alloy 617 did not develop protective oxide scales, and the creep properties of the alloy showed a decrease in life when compared with data generated in air. The aluminum content in Alloy 617 led to internal oxidation rather than an external scale, especially in environments with low oxygen partial pressure. It is believed that the impurity levels in gas-turbine based systems will be predominantly decarburizing since oxygen potential is expected to be much lower than that in steam-cycle based systems.

- Before materials performance can be assessed, it is essential to establish an operational window in terms of impurity levels in helium that can be maintained and controlled with certainty.

- Over the last 20 years, alloy manufacturers have developed several alloys with improved resistance to oxidation and to carburization/decarburization at elevated temperatures. These materials include Alloy 230, 602CA, microalloyed cast HP alloys, and W-containing Ni-base superalloys. It is beneficial to examine the scaling and corrosion performance of these alloys (in addition to Alloys 617, Hastelloy X, etc.) in helium with low oxygen partial pressures for their viability in the HTGRs.

- An extensive database is needed on candidate alloys for application in turbines (both for blades and disks), especially for direct-cycle systems.

Acknowledgments

This work is sponsored by the Office of Nuclear Regulatory Research, U.S. Nuclear Regulatory Commission, under Job Code Y6537; Senior Technical Advisor: J. Muscara; Program Manager: C. A. Greene. Figures 2.3 to 2.9, 3.9, 3.13, 3.14a, 3.18, and 3.21 in the report are reprinted with permission from the American Society for Mechanical Engineers, who is the original publisher of these figures. Figures 2.16 to 2.20, 2.22, 2.23, 3.6, 3.10, 3.11, 3.14b, and 3.15 in the report are reprinted with permission from the American Nuclear Society, who is the original publisher of these figures. Figure 6.2 in the report is reprinted with permission from General Atomics Company, who is the original publisher of the figure. The sources for various figures and their authors are identified in the report along with the figures.

1 Introduction

Development of the High Temperature Gas Reactor (HTGR) began in the 1950s, with significant advances in system design and fuel concepts during the 1960s and 1970s (IAEA 1990). The designs may be divided into two main groups, namely, steam-cycle HTGRs and modular-gas-turbine HTGRs. However, in all HTGR designs helium serves as the primary coolant. Table 1.1 lists the characteristics of selected steam-cycle HTGRs. In the steam-cycle HTGRs, helium from the primary circuit is used to produce steam, which in turn, drives the turbines to generate power. The early HTGR designs included Dragon, Arbeitsgemeinshaft Versuchsreaktor (AVR), and Peach Bottom, which utilized steel primary system vessels. The Dragon reactor incorporated graphite fuel elements containing particles coated by high-enriched-uranium carbide (Moore 1982). The core exit and inlet helium temperatures were 750 and 350°C, respectively.

In Germany, the 15 MWe AVR, a pebble-bed-type HTGR, began operation in 1967. The AVR had a steel containment vessel and used particle-fueled, graphite spheres 6 cm in diameter. The AVR operated with a core outlet temperature as high as 950°C (Kroger 1988). The Peach Bottom HTGR (40 MWe) in the U.S. operated without fuel failures for 897 equivalent full power days with fuel particles that were coated with isotropic pyrolytic carbon (Williams et al. 1994).

The subsequent HTGR plants, Fort St. Vrain (FSV) and the thorium high temperature reactor (THTR-300), had the primary systems enclosed in prestressed concrete reactor vessels (PCRVs). The FSV reactor was designed with a core of hexagonal, graphite-block fuel elements and reflectors with fuel in the form of ceramic-coated (TRISO) particles, once-through steam generator modules producing 538°C superheated steam, and steam-turbine-driven axial helium circulators (Moore 1982; Williams et al. 1994). The THTR-300 reactor, sponsored by Germany and Norway, was also based on the pebble bed concept. The plant was completed in 1984, and the reactor demonstrated the desired safety characteristics, control response of the pebble bed, and good fission product retention of the fuel elements before it was shut down permanently in 1991. The designs discussed above are all based on steam plants for power generation.

The advanced HTGR concept currently considered by the Member States of the IAEA's International Working Group on Gas Cooled Reactors (IWGGCR) involves a closed-cycle gas turbine for power generation with a core outlet/gas turbine inlet temperature of 850°C and a net plant efficiency of 47% (Cleveland et al. 1997). Table 1.2 lists the characteristics of various gas-turbine based HTGRs. In these designs, the helium from the core is used directly to drive the turbines or indirectly to heat the air or nitrogen, which drives the turbines. The system concepts include the Gas Turbine-Modular Helium Reactor (GT-MHR) pursued by a consortium led by General Atomics in the U.S., the Pebble Bed Modular Reactor (PBMR) designed by ESKOM of South Africa and British Nuclear Fuels of U.K., and the High Temperature Engineering Test Reactor (HTTR) of Japan.

The main focus of this report is to evaluate the materials performance and long-term behavior in environments typical of gas-turbine based HTGRs. As a part of this evaluation, the materials that have been used in HTGRs, their functions, and the environmental conditions under which they have operated are identified. The materials to be used in new HTGRs, the

Table 1.1 Characteristics of selected steam cycle HTGRs
(Boyer et al. 1974, Brey 2000, Nickel 1989)

	AVR	Peach Bottom	Ft. St. Vrain	Fulton	THTR-300	HTR-500	VGM-400	HTR-Module	MHTGR
Country of Origin	Germany	U.S.	U.S.	U.S.	Germany	Germany	Russia	Germany	U.S.
Thermal Power, MWt	46	115	842	2,979	750	1,390	1,060	200	350
Net. Electric Power, MWe	13	40	330	1,160	300	550	Co-Gen.	80	139
Core Outlet Temp., °C	950	725	775	741	750	700	950	700	686
Helium Pressure, MPa	1.1	2.25	4.8	5.0	3.9	5.5	5.0	6.6	6.4
Steam Temp., °C	505	538	538/538	513	530/530	530	535	530	538
Reactor Type	Pebble	Sleeve	Block	Block	Pebble	Pebble	Pebble	Pebble	Block
Vessel Material	Steel	Steel	PCRV*	PCRV	PCRV	PCRV	PCRV	Steel	Steel
Date of Operation	1966	1967	1979 to 1989	No operation	1985	No operation	No Data	No operation	No operation

*Prestressed concrete reactor vessel.

Table 1.2 Characteristics of selected modular HTGR gas turbine plants* (Brey 2000)

	GT-MHR	PBMR	MHTGR-IGT	ACACIA	GTHTR-300	HTR-GT 600MW	MPBR
Country of Origin	U.S./Russia	S. Africa	China	Netherlands	Japan	Japan	U.S.
Thermal Power, MWt	600	265	200	40	600	600	250
Net. Electric Power, MWe	278	116	~96	Co-Gen.	273	287	112
Core Outlet Temp., °C	850	900	900	800	850	850	850
Helium Pressure, MPa	7.15	7.0	6.0	2.3	6.8	6.0	7.9
Cycle Type (Secondary Coolant)	Direct	Direct	Indirect (nitrogen gas)	Direct	Direct	Direct	Indirect (air)
Core Type	Block	Pebble	Pebble	Pebble	Block	Pin/Block	Pebble
Vessel Material	Mod 9Cr1Mo	SA 508	SA 516-70	Steel	SA 508	Mod 9Cr1Mo	Steel

*The systems were either planned or designed, but none was constructed.

functions they will serve, and the anticipated environmental conditions under which they are expected to operate are likewise identified. Those HTGR conditions that may affect material property response, such as the steady-state operating environment, component geometry, and off-normal conditions, are discussed and evaluated.

1.1 Gas Turbine Modular Helium Reactor

The GT-MHR is an advanced gas-cooled reactor under development in a joint United States-Russian Federation program. The GT-MHR is designed with the potential for substantial improvements in the areas of safety, thermal efficiency, and environmental advantage when compared with designs developed in the 1980s. The GT-MHR module, shown in Figure 1.1, couples a gas-cooled modular helium reactor (MHR), contained in one vessel, with a high-efficiency Brayton cycle gas turbine (GT) contained in a second vessel. The reactor and power conversion vessels are interconnected with a short cross-vessel, and both the vessels are located in a below-grade concrete silo.

Key features of the gas-cooled MHR are the helium coolant, graphite moderator, and refractory-coated particle fuel. The helium coolant is relatively inert, the graphite moderator has high strength and stability to high temperatures, and the refractory-coated fuel particle retains the fission products to high temperatures. The helium coolant is heated in the reactor core by flowing downward through the coolant channels in graphite fuel elements and then through the cross-vessel to the power conversion system. The power conversion system contains a gas turbine, an electric generator, and gas compressors on a common, vertically oriented shaft supported by magnetic bearings. The power conversion system also includes the recuperator, precooler, and intercooler heat exchangers. Table 1.3 lists the component materials for GT-MHR plant and their operating environments.

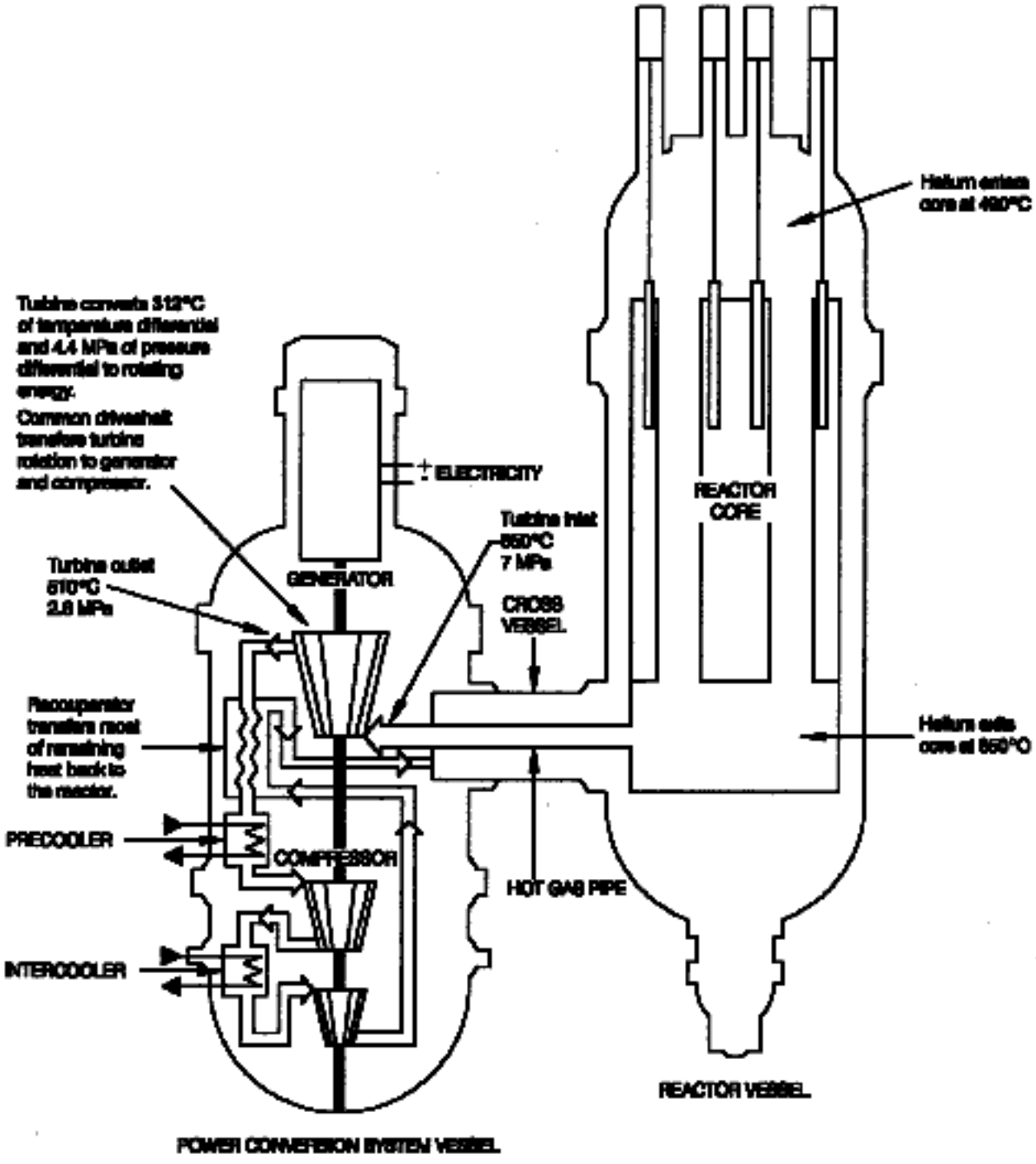

Figure 1.1 Schematic of gas turbine-modular helium reactor (GT-MHR)

Table 1.3 GT-MHR component materials

Components	Environment	Material	Comments	References	Code Status
Reactor Pressure Vessel Cross-Vessel	Normal operating temperature 290°C Pressure ~7.07 MPa	SA 508 GR3, Cl1 SA 508 Class 1 SA 533 Grade B, Class 1	Insulated vessel design or vessel cooled by helium returning from turbine	EPRI 2002 Shenoy and Betts 1988; Muto et al. 2000; Buckthorpe et al. 2002	ASME Code Case N-499-1
	Normal operating temperature ~ 500°C	9Cr-1Mo-V (also called modified 9Cr1Mo) (10X9MFB in Russia)	This material is not yet authorized as the Class 1 vessel material. Mod 9Cr1Mo has a big advantage over 2.25Cr1Mo above 450°C; limited data for as-received and post weld heat-treated base material and weldments; limited fabrication experience. Tests scheduled to begin mid 2002.	Muto et al. 2000 IAEA 2001 Buckthorpe et al. 2002 Kiryushin et al. 1997	None available
Reactor System Metallic Components - core support structure - reactor internals	Core inlet/outlet temperatures 491/850°C	2-1/4 Cr-1 Mo Type 316 SS Alloy 800H Alloy 617 Hastelloy X	The support structure includes the upper support plate, core barrel shell, gas duct shell, bottom collector header shroud, hot duct nozzle, and the shutdown cooling system header. The reactor internals include top collector plenum and its shroud, hot duct assembly, control rod canister, plenum element casing, and core lateral restraint.	LaBar 2002; Shenoy and Betts 1988 EPRI 2002 IAEA 2001 Natesan et al. 2003	ASME Code Case N-201-4 (Maximum allowable temperatures of 816°C or lower – See Table 5) ASME Draft Code Case for Alloy 617 (Maximum allowable temperature of 982°C)
Shutdown Cooling System (SCS) - conical shell - bottom - gas circulator	850°C (conical shell) 490°C (bottom and gas circulator)	Alloy CrNi55MoWZr (conical shell) Type 321 SS (gas circulator blades)		EPRI 2002	None available
Reactor Core Cooling System (RCCS) Component	490°C	Type 321 SS		EPRI 2002	None available

Table 1.3 GT-MHR Component Materials (continued)

Components	Environment	Material	Comments	References	Code Status
Hot Gas Pipe	850°C	Alloy 617			ASME Draft Code Case for Alloy 617 (Maximum allowable temperature of 982°C)
Power Conversion System (PCS) Vessel	150°C	15X2NMFA (in Russia) 15Cr2NiMoVN		Kiryushin et al. 1997 EPRI 2002	ASME Section III, Subsection NB
Recuperator (including heat exchange surface)	Helium parameters for low/high pressure side: - Inlet 507.5°C, 2.63 MPa /108.1°C, 7.22 MPa - Outlet 127.3°C, 2.60 Mpa /487.5°C, 7.15 MPa	Austenitic stainless steel 08Cr16Ni11Mo3		IAEA 2001	ASME Section III, Subsection NH (Maximum allowable temperatures of 816°C or lower – See Table 5)
Precooler and Intercooler	150°C (He) 60°C (air)	Type 321 SS		EPRI 2002	ASME Section III, Subsection NB

1.2 Pebble Bed Modular Helium Reactor

The PBMR is a helium-cooled, graphite-moderated, high-temperature reactor, a schematic of which is shown in Figure 1.2. The PBMR design is aimed at achieving a plant that has no physical process, however unlikely, that could cause a radiation-induced hazard outside the site boundary (IAEA, 2001). This is principally achieved in the PBMR by demonstrating that the integrated heat loss from the reactor vessel exceeds the decay heat production in the post-accident condition, and that the peak temperature reached in the core during the transient is below the demonstrated fuel degradation point and far below the temperature at which the physical structure is affected.

The metallic parts in the core structure include the core barrel with its bottom support structure, support flange at the lower section and stiffening ring at the top, helium flow channels, pipes and components of the fueling system, fueling tube, and lower discharge tube. The power conversion unit converts the heat from the reactor into electrical energy via a Brayton cycle. The turbine inlet temperature is 900°C. A thermal power level of 265 MW is calculated to provide a gross electrical generation of 117 MWe. Helium, at a pressure of 7.0 MPa and a temperature of 900°C, leaves the pebble bed reactor and flows through the high- and low-pressure turbines, providing energy to drive their compressors. The helium, at 721°C and 4.4 MPa, then enters the power turbine, providing energy to drive the electrical generator. The helium at 554°C then enters the recuperator, which provides heat exchange to the helium returning to the core. After leaving the recuperator at 140°C, the helium passes through the precooler and exits the cooler at 27°C and 2.6 MPa. Before entering the high pressure side of the recuperator, the helium is then compressed by passing through the low-pressure compressor, intercooler, and then the high-pressure compressor. The recuperator heats the helium from 104°C to 536°C at a pressure of 7.0 MPa before it enters the top of the reactor.

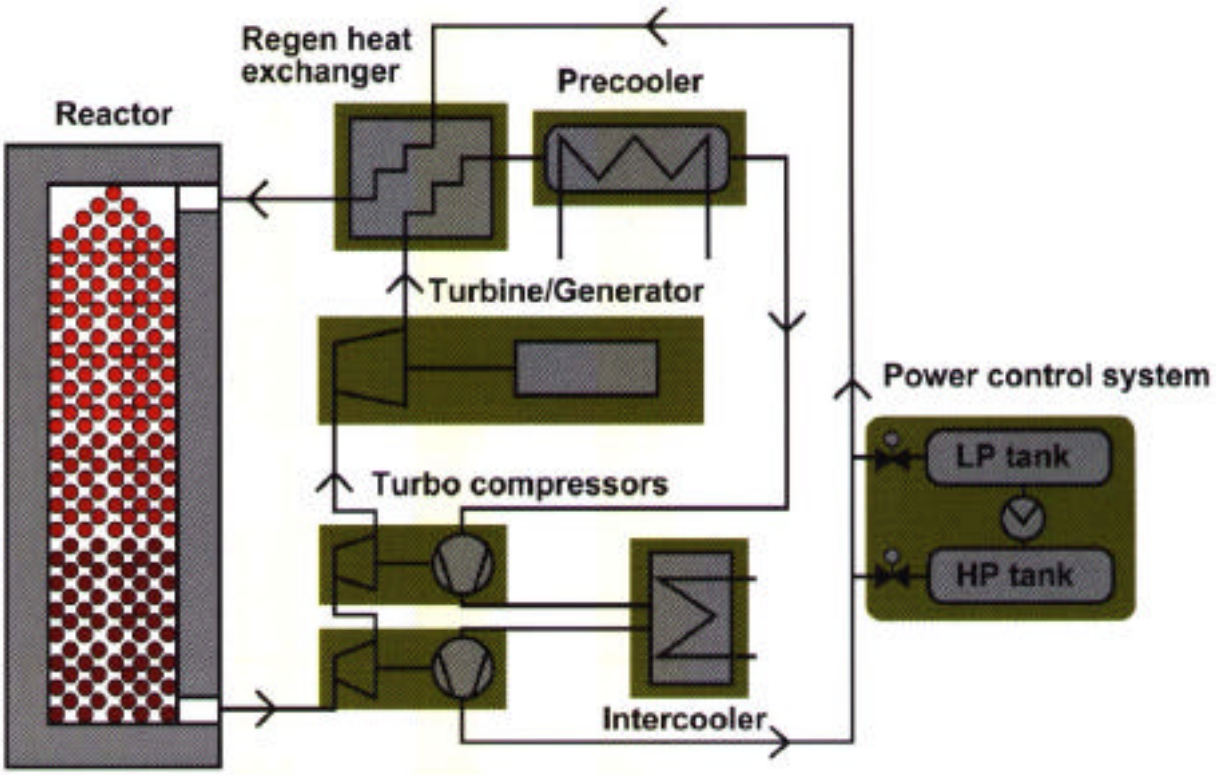

Figure 1.2 Schematic of pebble bed modular helium reactor (PBMR)

2 Metallic Components

The primary helium coolant in the gas-turbine based HTGRs is expected to be at temperatures in the range of 850-900°C, and the selected materials should have adequate performance over long service life at temperatures in the range of 900-950°C. There are several key issues in materials selection for such an application, and reliable component performance requires a significant database for the selection of materials and for assessment of the long-term effects on the materials behavior in the service environment. This report reviews the literature on HTGR materials properties and the environmental effects on the behavior of metallic materials. The technical issues addressed in this report are:

- Baseline mechanical property data developed in an air environment,
- Effects of helium coolant chemistry on materials degradation,
- Helium purification and control,
- Corrosion effects on mechanical properties of candidate materials,
- Fission product release and its effect on materials,
- Corrosion-erosion due to particulate-laden gas flow, and
- Design methodology.

2.1 Structural Materials

In this section, baseline mechanical property data are presented for several candidate materials that are being considered for application in HTGRs. The properties include tensile, creep rupture, low-cycle fatigue, creep-fatigue, and fracture toughness. The information is discussed to assess the adequacy and applicability of data for the design of components in HTGR environments with long service life. The availability and adequacy of design codes, rules, and procedures for various components are discussed in a companion report (Shah et al. 2003).

Among the materials, 2 1/4Cr-1Mo and modified 9Cr-1Mo ferritic steels are considered for application in reactor pressure vessels. Fe-Cr-Ni alloys such as Alloy 800H and austenitic stainless steels are considered for recuperators and reactor internals. Alloys such as 617, Hastelloy X, and Hastelloy XR are considered for components that will be exposed to helium coolant at temperatures up to 900°C. Alloys such as 713LC and Mo-TZM are considered for turbine blades. Alloys such as A286, 706, and 718 are examined for turbine disk applications. Table 2.1 lists the nominal chemical compositions of several candidate alloys along with their potential applications in HTGR components.

2.1.1 2.25Cr-1Mo Ferritic Steel

A substantial database is available on the tensile, creep, fatigue, and creep fatigue properties for 2.25Cr-1Mo ferritic steel. In addition, this database includes the effect of long-term aging on microstructural changes and mechanical properties at temperatures of interest for pressure vessel application in HTGRs. Furthermore, the material has been ASME-code

Table 2.1 Nominal chemical composition (in wt.%) of candidate alloys and their application

Material	C	Cr	Ni	Co	Mo	Ti	Al	Fe	Other	Application
2.25Cr-1Mo	0.20	2.3	-	-	1.0	-	–	Bal[a]	–	Pressure vessel
9Cr-1Mo	0.08	8.6	-	-	1.0	-	-	Bal	V 0.2, Nb 0.07	Pressure vessel
HT 9	0.2	12	0.3	-	1	-	-	Bal	V 0.25, W 0.5	Pressure vessel
316 SS	0.05	18	14	-	2.2	-	-	Bal	–	Recuperator
800H	0.08	20.1	31.7	-	0.3	0.4	0.4	Bal	–	Piping, internals
Hastelloy X	0.1	21.5	Bal	2.0	9.0	-	-	18.5	W 0.6	Piping, internals
617	0.06	21.6	53.6	12.5	9.5	0.3	1.2	0.9	–	Piping, internals
Hastelloy-XR	0.07	22	Bal	0.04	9.1	-	-	18.2	W 0.5, Mn 0.9,	Piping, internals
Nimonic-86	0.07	25	Bal	-	10	0.1	-	1.7	–	Piping, internals
Hastelloy S	0.02	15.5	Bal	-	14.5	-	0.2		–	Piping, internals
Manaurite	0.4	25	35	-	-	-	-	Bal	Nb 1	Piping, internals
Inconel 519	0.3	24	24	-	-	-	-	Bal	Nb 1	Piping, internals
713LC	0.07	12	Bal	-	5	0.7	6	-	Nb 2, Zr 0.1	Turbine blades
Mar-M 004	0.07	12	Bal	-	4.5	-	6	-	Hf 1.3, Nb 1.6, Ta 0.3	Turbine blades
M21	0.1	6	Bal	-	2	-	6	-	W 10.5, Nb 1.5, Zr 0.1	Turbine blades
738	0.11	16	Bal	9.0	2	-	3.4	-	W 2.6, Ta 2, Nb 0.9	Turbine blades
Udimet 520	0.05	19	Bal	12.0	6	3.0	2	-	W 1	Turbine blades
Mo-TZM	0.02	-	-	-	Bal	0.5	-	-	Zr 0.8	Turbine blades
A286	0.05	15	26.0	-	1.3	2.5	0.2	Bal	B 0.015	Turbine disks
706	0.03	16	42.0	-	0.5	1.0	0.2	Bal	Nb 2.9	Turbine disks
718	0.1	19	Bal	-	3	0.8	0.6	19	Nb 5.2	Turbine disks
Waspaloy	0.08	20	Bal	13.5	4.3	3.0	1.3	-	Zr 0.06	Turbine disks
Udimet 720	0.03	18	Bal	14.5	3	5.0	2.5	-	W 1.3	Turbine disks
MA 6000	0.05	15	Bal	-	2	2.5	4.5	-	W 4, Ta 2, Y_2O_3 1.1	Turbine disks

[a]Indicates balance.

certified for application in nuclear systems. This report will not include a discussion of this well-established database.

2.1.2 Modified 9Cr-1Mo Ferritic Steel

The 9Cr-1Mo-V steel is a modified alloy system similar to conventional 9Cr-1Mo grade ferritic steel. Modifications include additions of vanadium, niobium, and nitrogen, as well as lower carbon content. This alloy is much more resistant to thermal fatigue than austenitic stainless steels because of its lower thermal expansion coefficient (at least 30% lower) and higher thermal conductivity. This alloy provides extremely good mechanical properties at elevated temperature when produced and heat treated to form the proper microstructure. This microstructure includes stable submicroscopic vanadium-rich $M_{23}C_6$ particles that contribute to high-temperature strength and creep resistance (Brush 2001).

Table 2.2 presents the chemical composition of three additional grades of 9Cr-1Mo-V steels along with Grade P9 steel. The steel designated P91 was developed at Oak Ridge National Laboratory (Sikka et al. 1981). It shows a remarkable increase in stress rupture strength, achieved by addition of 0.2 V, 0.06 Nb, and 0.05 N. The steel designated P92 was developed at Nippon Steel, in which a further increase in stress rupture strength was obtained by addition of 1.8% W and reduction of the Mo content from 1 to 0.5%. Similar steel, designated E911, was developed in a European program. This steel contains 1% Mo and 1% W and offers stress rupture strength similar to P92. This development of 9Cr-1Mo-V steels is illustrated in Figure 2.1, which shows the 100,000-h stress rupture strength of Grades P9, P91, P92, and E911 at 600 and 650°C.

Table 2.2 Chemical composition (in wt%) of several grades of 9Cr-1Mo steels

Element	P9	P91	P92	E911
C	Max. 0.15	0.10	0.124	0.105
Si	0.20-0.65	0.38	0.02	0.20
Mn	0.80-1.30	0.46	0.47	0.35
P	Max. 0.030	0.020	0.011	0.007
S	Max. 0.030	0.002	0.006	0.003
Cr	8.5-10.5	8.10	9.07	9.16
Mo	1.70-2.30	0.92	0.46	1.01
W	--	--	1.78	1.00
V	0.20-0.40	0.18	0.19	0.23
Nb	0.30-0.45	0.073	0.063	0.068
B	--	--	0.003	--
N	--	0.049	0.043	0.072
Ni	Max. 0.30	0.33	0.06	0.07
Al	--	0.034	0.002	--
Heat treatment		1 h at 1050°C + 1 h at 750°C, air cool	2 h at 1070°C + 2 h at 775°C, air cool	1 h at 1050°C + 1 h at 750°C, air cool
100,000-h stress rupture strength at 600°C (MPa[a])	35	94	115	110

[a]Values for P91 from Canonico (1994), for P92 from Wachter et al. (1995), and for E911 from Staubli et al. (1998).

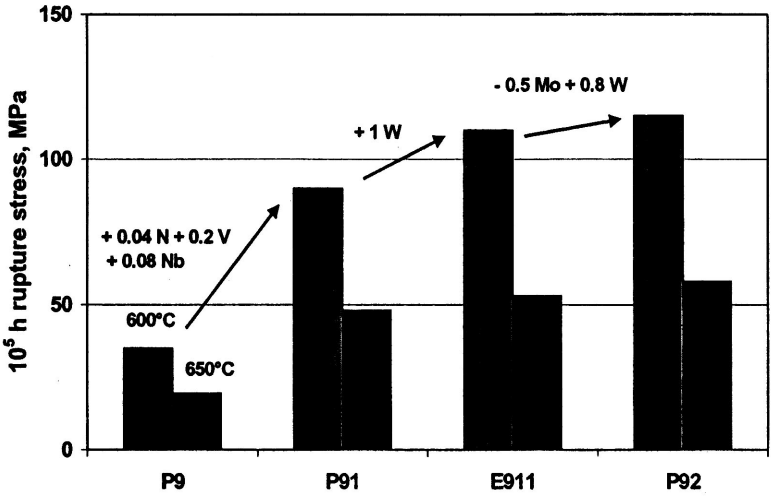

Figure 2.1 Rupture stress in development of 9%Cr steels (Sikka et al. 1983).

Extensive studies (Sikka et al. 1981, Brinkman et al. 1990, Swindemann et al. 1998) have been conducted on a nominally Fe-9Cr-1Mo class of ferritic steels to evaluate their tensile, creep rupture, and low-cycle fatigue properties. Long-term aging effects on the mechanical properties have been determined with this material (Swindeman et al. 2000). Figure 2.2 shows the secondary creep rates of P91, P92, and E911 at 600 and 650°C plotted against the applied stress. In the high stress region, the differences in the secondary creep rates of the three steels are relatively small, whereas the differences between the steels become more pronounced in the low stress region. The creep deformation characteristics may be described by the Norton equation with two values of Norton's stress exponent *n*. At high stresses, the value of *n* is

around 16, whereas at low stresses, it is 6. The change in *n* indicates a change in the creep characteristics.

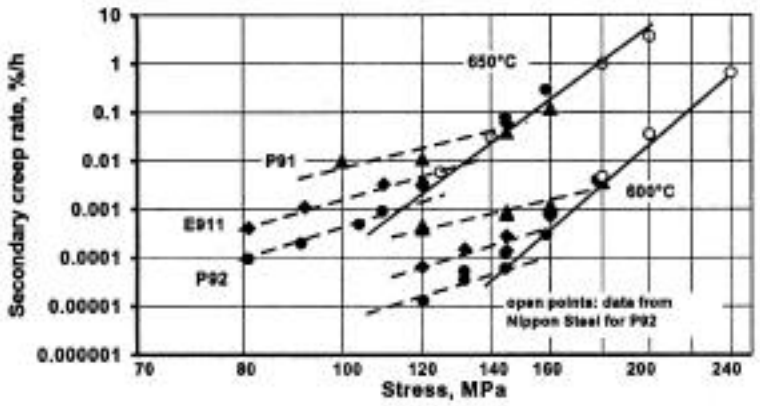

Figure 2.2 Secondary creep rates for P91, P92, and E911 (Ennis and Czyrska-Filemonowicz 2002).

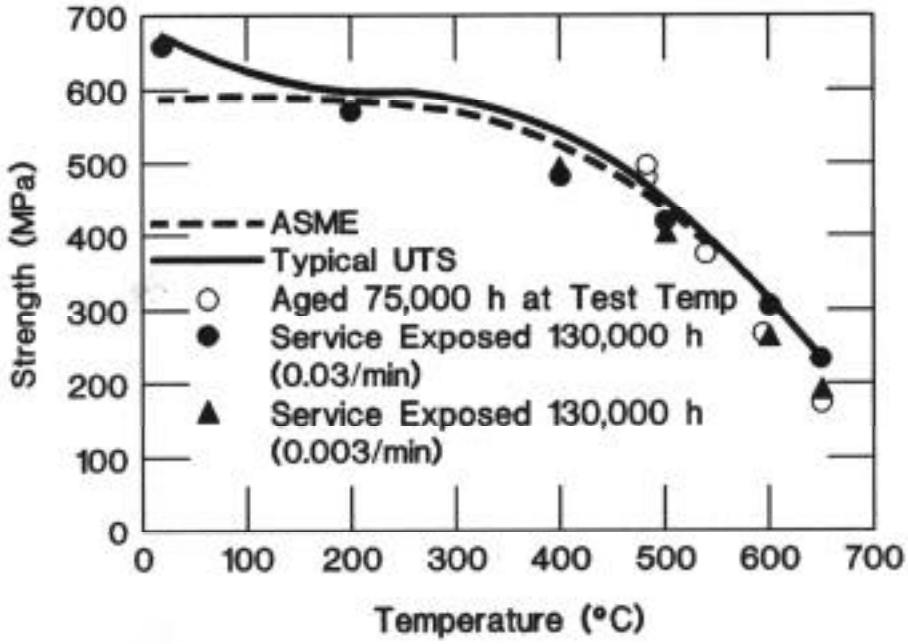

Figure 2.3 Comparison of ultimate tensile strength of unexposed Grade 91 with aged and service-exposed materials (Swindeman et al. 2000).

Figure 2.3 shows the ultimate tensile strength after long-time aging, which is compared to a trend curve for unexposed material. Plates aged for 75,000 h were tested at the aging temperature. For aging at 482°C (900°F), little effect was noticed. If anything, a slight increase in strength was observed. The ultimate strength at 649°C (1200°F) was significantly below the trend curve for typical material. A more detailed analysis of the influence of aging time and temperature is reported elsewhere (Brinkman et al. 1990). The material exposed to service conditions for 130,000 h was tested at several temperatures. It was reported that the strength fell below the trend curve for typical as-tempered material. At a comparable strain rate, the strength of the service-exposed material was similar to the aged material at 593 and 649°C (1100 and 1200°F).

Creep curves for service-exposed and unexposed modified 9Cr-1Mo steel are shown in Fig. 2.4 for tests conducted at 600°C (1112°F) and 100 MPa (14.5 ksi). The service-exposed material exhibited a creep rate that was ten times greater than the unexposed steel.

The unexposed material remained in the primary creep stage to beyond 15,000 h. Creep curves for the service-exposed Grade 91 tested at different temperatures are shown in Fig. 2.5. For 100 MPa, the creep rates at 625 and 600°C (1157 and 1112°F) accelerate around 1% strain, whereas the creep rates at 575 and 550°C (1067 and 1022°F) showed no acceleration around 1% strain after 20,000 h. The minimum creep rates at 100 MPa (14.5 ksi) for three aging conditions are compared to the unexposed behavior in Fig. 2.6. These data are plotted against the reciprocal of absolute temperature, and the trend indicates activation energy as well as relative creep strength. The steeper slopes indicate higher activation

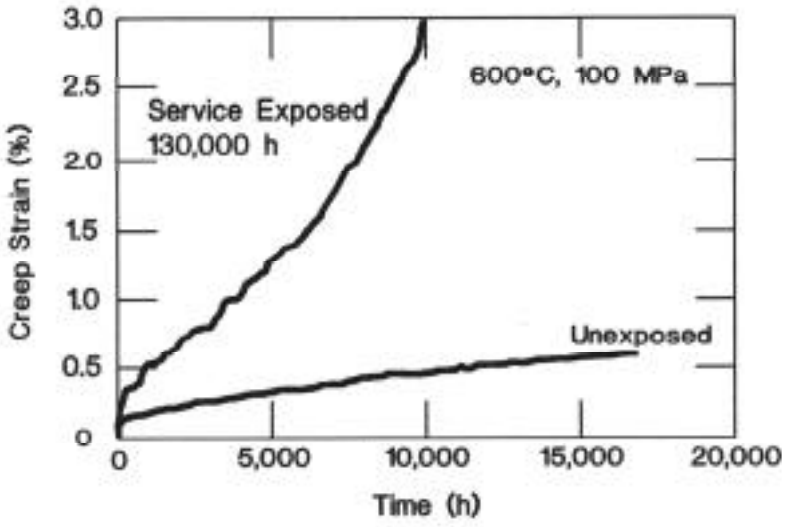

Figure 2.4 Comparison of creep curves for unexposed and service-exposed Grade 91 at 100 MPa (Swindeman et al. 2000).

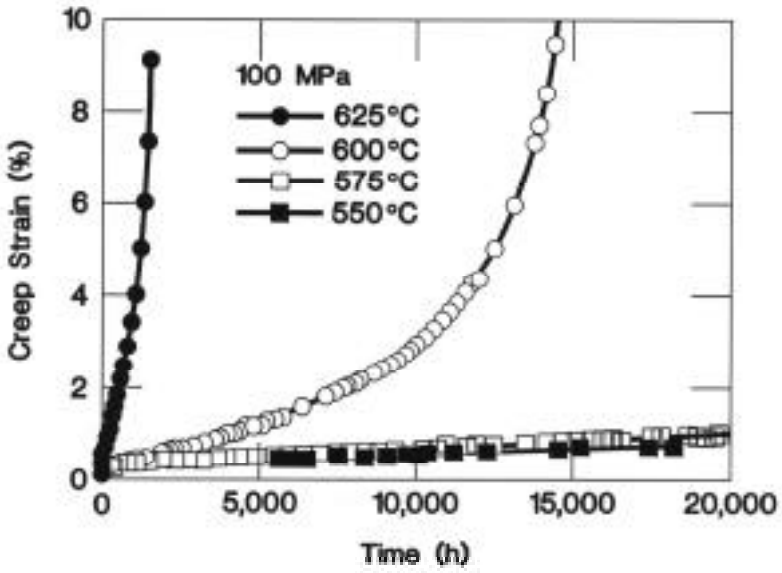

Figure 2.5 Creep curves for service-exposed Grade 91 at 100 MPa and several temperatures (Swindeman et al. 2000).

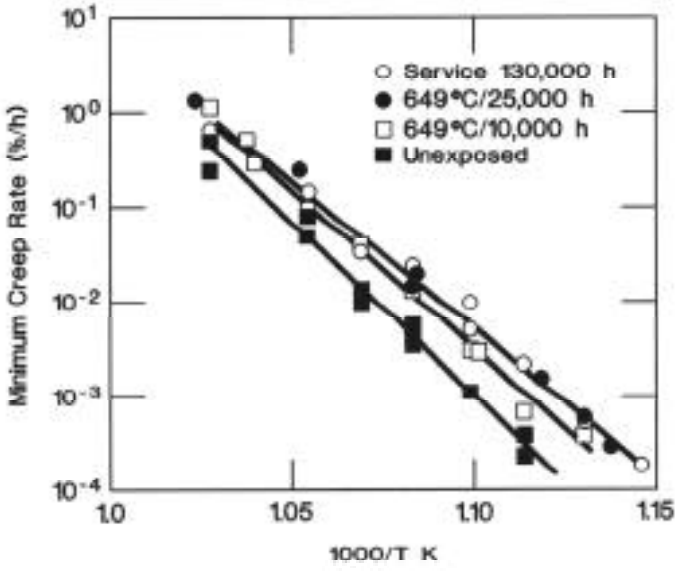

Figure 2.6 Comparison of isostress plots of minimum creep rate of Grade 91 for several material conditions at 100 MPa (Swindeman et al. 2000).

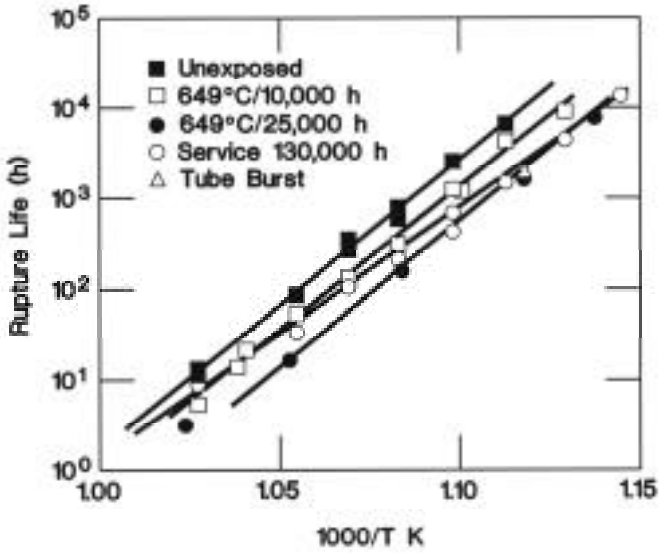

Figure 2.7 Comparison of isostress plots of rupture life of Grade 91 for several material conditions at 100 MPa (Swindeman et al. 2000).

energies. The lowest value for reciprocal temperature corresponds to the highest temperature of testing (700°C). With decreasing test temperature (increasing reciprocal temperature), data tended to diverge. The service-exposed material exhibited the highest creep rate, and the data for material aged 25,000 h at 649°C mingled within the trend. Material aged 10,000 h at 649°C exhibited lower creep rates, whereas the unexposed material exhibited the lowest rates.

For any temperature, the creep rates for all conditions varied by less than a factor of ten. The slopes of the lines drawn through the data indicated that the activation energy for creep of the service-exposed material was lower than that for the unexposed material. A plot of rupture life versus the reciprocal temperature for the 100 MPa isostress data is shown in Fig. 2.7. With the exception of one short-time test result on material aged 25,000 h at 649°C, the aged and unexposed materials exhibited the same temperature dependence. The unexposed material had the longest life, and material aged 25,000 h at 649°C had the shortest. The service-exposed material showed a different temperature dependence. The slope of the line drawn through the data indicated lower activation energy for rupture than the unexposed material.

The rupture lives for different conditions varied by less than a factor of ten at any temperature examined. The rupture life of the pressurized tube was included in the plot, and the point fell on the trend for the uniaxial tests.

Although the temperature dependence of the rupture life of service exposed material appeared to differ from that for the aged materials, the Monkman-Grant correlation for all conditions was similar. Data for several heats of unexposed material are compared to the aged and service-exposed materials in Fig. 2.8. All data follow the same trend. As is often the case, the trend for the long-time data was not as well defined as shorter time data. Rupture data for more than forty tests on aged and service-exposed materials are plotted in Fig. 2.9 as stress versus the Larson Miller parameter. A parametric constant of 30 was selected for the correlation. Included in the plot are rupture data for a large number of tests on unexposed material. Results clearly show that the rupture lives for the aged and service-exposed materials fell near the lower strength or shorter life side of the scatter band for the unexposed material. At the higher values of the Larson Miller parameter, the strength of the severely aged materials was reduced to about 80% of the average for the unexposed material.

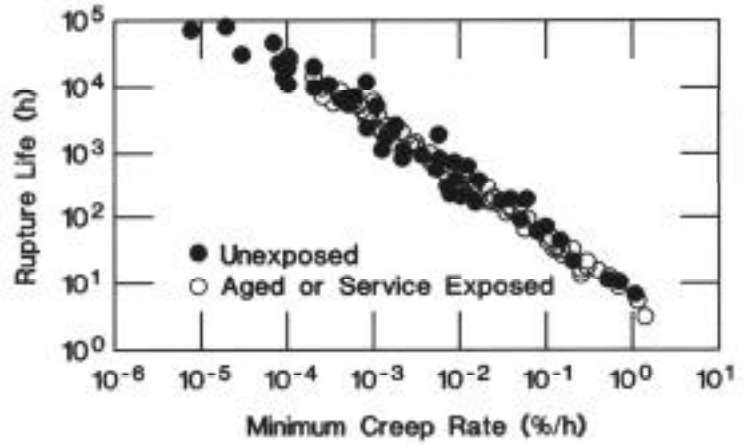

Figure 2.8 Monkman-Grant plot for unexposed, aged, and service-exposed Grade 91 steel (Swindeman et al. 2000).

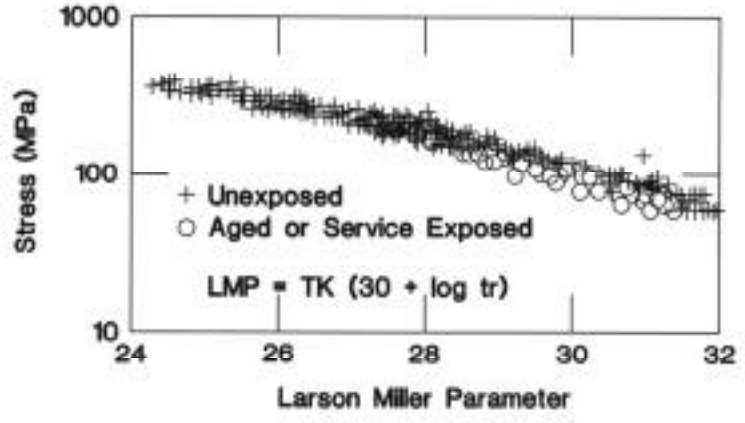

Figure 2.9 Stress versus Larson-Miller parameter for unexposed, aged, and service-exposed Grade 91 steel (Swindeman et al. 2000).

Monkman-Grant, isostress, and Larson-Miller correlations were used to describe the strength of the material with aging in service in the temperature range of interest for pressure vessel applications (Figs. 2.8 and 2.9). Changes in strength were attributed to coarsening of the metallurgical substructure of the tempered martensite in the material (Swindemann et al. 2000).

Low-cycle fatigue behavior of modified 9Cr-1Mo steel has been evaluated in several studies (Hoffman 1982, Jones 1983, and Ebi and McEvily 1984). The cyclic stress-strain curves at 50% of the number of cycles to failure are shown in Fig. 2.10 (Ebi and McEvily 1984). The results indicate a higher cyclic strength for the hot-rolled material compared with that for the hot-forged material. Also included in Fig. 2.10 are correlations that relate cyclic stress and cyclic strain. Ebi and McEvily (1984) also measured fatigue crack propagation rate as a function of crack length by measuring the fatigue striation spacing on the failed test specimens. They concluded that the crack propagation rate was similar for both the hot-rolled and hot-forged materials when tested in air (see Fig. 2.11). But they reported that the crack growth rates were lower in vacuum than in air for the hot-rolled material.

9Cr-1Mo-V materials have been adopted in various forms in a number of ASTM/ASME standards. Many are listed in the ASME Boiler and Pressure Vessel Code Section II, Part D, allowable stress tables with a maximum temperature rating of 649°C (1200°F) for ASME Code Section I and Section VIII, Division 1, and rating of 371°C (700°F) for Section III, Class 1, 2, and 3.

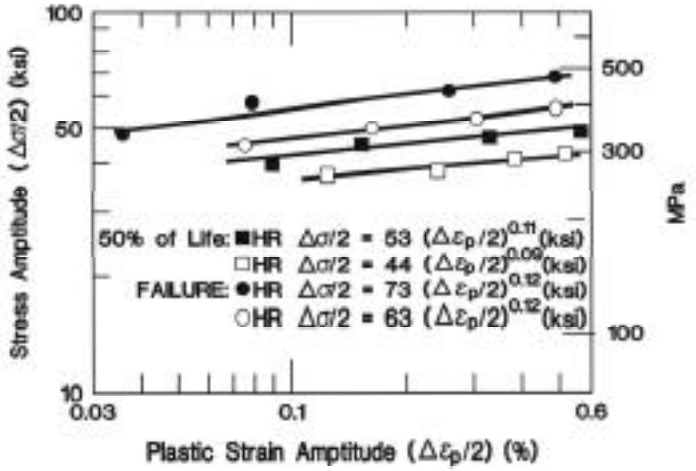

Figure 2.10 Cyclic stress-strain properties of hot-rolled and forged materials of modified 9Cr-1Mo steel (Ebi and McEvily 1984).

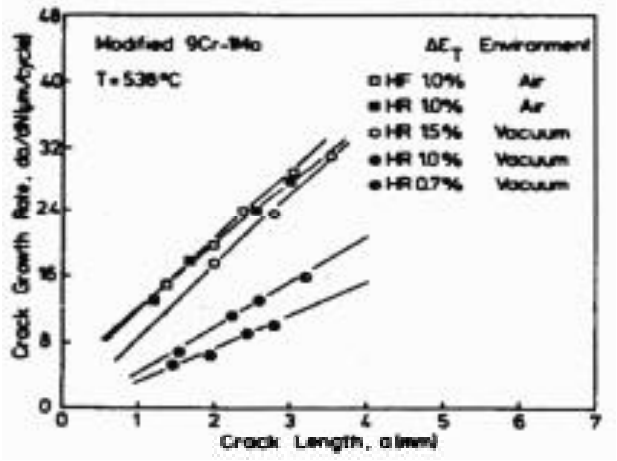

Figure 2.11 Fatigue crack propagation rate as a function of crack length for modified 9Cr-1Mo steel (Ebi and McEvily 1984).

2.1.3 Alloy 800H

Alloy 800H consists of Fe-Cr-Ni with a minimum carbon content of 0.05 wt.% and a grain size of ASTM No. 5 or coarser. This alloy must be solution annealed at ≈1093°C, has stable austenitic structure, and is intended for use at temperatures >593°C. Both the high carbon content and the high solution-anneal temperature promote a large stable grain size, which provides better creep properties. This alloy is currently approved under ASME Code for nuclear service up to 760°C.

The material is free of precipitates in the solution-annealed condition. After long times at a service temperature of ≈550°C, γ' precipitates tend to form. These precipitates can reduce the creep ductility of the alloy (Betteridge et al.1978). To minimize the decrease in creep ductility, the volume fraction of γ' precipitates is controlled by specifying a concentration limit of ≈0.8 wt.% for the Al + Ti content in the alloy. The minimum creep rate for the alloy at elevated temperatures is depicted by Norton's law and the Arrhenius function, as follows (Blackburn 1972):

$$\dot{\varepsilon}_m = \text{constant}(\sigma/E)^n \exp(-Q/RT) \quad (1)$$

where σ, E, Q, R, and T are applied stress, elastic modulus, activation energy, gas constant, and absolute temperature.

Figure 2.12 shows the allowable stress values S_{mt} used for primary general membrane calculations for actual service life and for normal-plus-upset conditions, as specified by ASME boiler and pressure vessel code (ASME 1977). Figure 2.13 shows the minimum creep rate

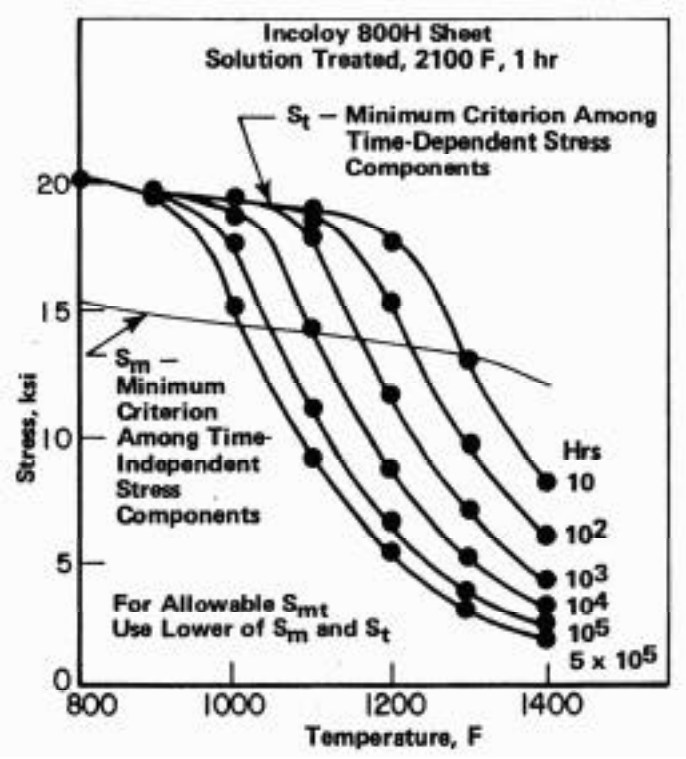

Figure 2.12 Allowable stress values S_{mt} for primary membrane calculations for actual service life and for normal-plus-upset conditions, as specified by ASME Boiler and Pressure Vessel Code (ASME 1977).

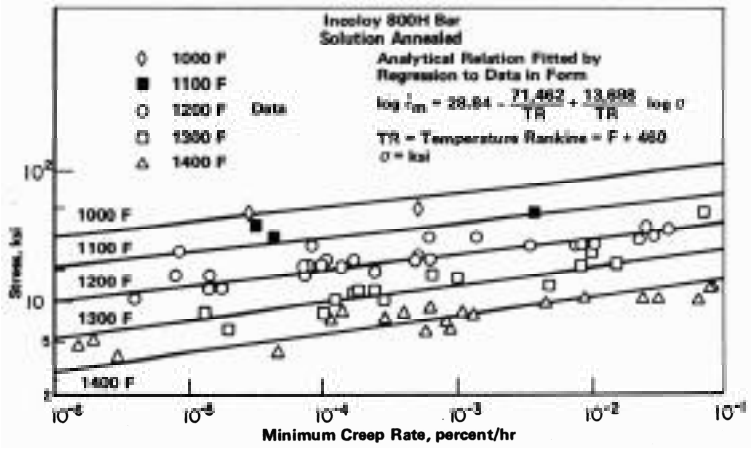

Figure 2.13 Minimum creep rate versus stress at 538-760°C (1000-1400°F) and correlations developed by regression analysis (Booker et al. 1978).

versus stress at 593 to 760°C, with comparison to results derived by regression analysis (Booker et al. 1978). Fatigue behavior of Alloy 800H has been evaluated from room temperature to 760°C (Soo and Chow 1976, Soo and Chow 1978, Chow et al. 1978). Figure 2.14 shows low- and high-cycle fatigue data (typical of information available) for Alloy 800H at 760°C, plotted as log-log plots of elastic and total strain range versus life.

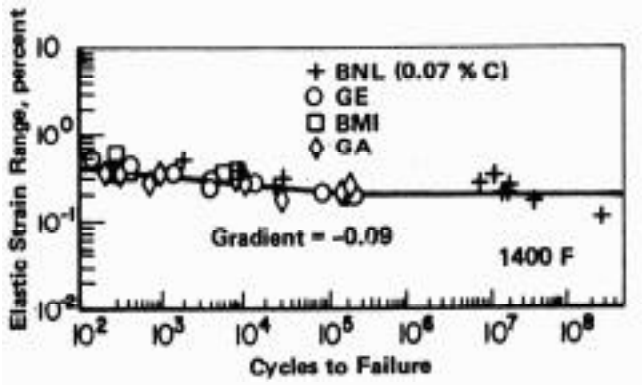

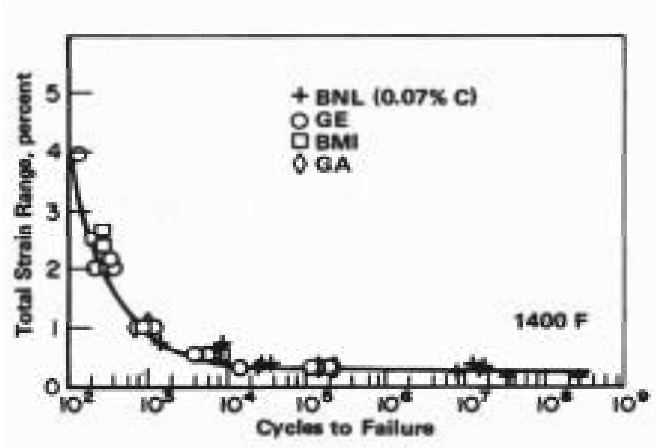

Figure 2.14 Low- and high-cycle fatigue behavior of Alloy 800H at 760°C (Soo and Chow 1978). BNL, GE, BMI, and GA in the figures refer to Brookhaven National Laboratory, General Electric Company, Battelle Memorial Institute, and General Atomics Company, respectively.

2.1.4 Alloy 617, Hastelloy X, and Other Alloys

The alloys discussed in this subsection are selected for service at temperatures in excess of 750°C, and the components fabricated from these alloys will be subjected to exposures at elevated temperatures to helium coolant with potential impurities. This subsection will address the elevated-temperature mechanical properties of candidate alloys, and the effects of helium coolant will be addressed in Section 3.

Alloy 617 is an austenitic alloy based on nickel-chromium with further alloying additions of cobalt, molybdenum, and aluminum. The alloy has exceptional creep strength at temperatures above 870°C, enhanced by solution strengthening from the molybdenum and cobalt additions. It has good cyclic oxidation and carburization resistance, imparted by the chromium and aluminum additions. The alloy retains toughness after long-time exposure at elevated temperatures; it does not form embrittling phases such as sigma, mu, chi, or Laves. It has good weldability and lower thermal expansion than most austenitic stainless steels. As a result, the alloy has been extensively studied for application at elevated temperatures in HTGRs.

Tensile properties of Alloy 617 and Hastelloy X in solution-annealed and aged conditions were evaluated by Strizak et al. (1982), and the results are shown in Fig. 2.15. Several studies have been conducted to evaluate the creep and rupture properties of Alloy 617 at temperatures >650°C (Schubert et al. 1984, Tanabe et al. 1984, Cook 1984, Schneider et al. 1984, Osthoff et al. 1984). A database has been developed for the alloy that includes (1) the creep properties such as time for 1% strain and time to rupture, (2) the correlation between secondary creep rate and applied stress, and (3) correlations using the Larson Miller parameter to depict time for 1% creep strain and rupture as functions of test time and temperature. Data have been generated up to test times of 20,000 h and in multiple heats of the alloy. Figure 2.16 shows the experimental data on 1% creep strain as a function of applied stress at temperatures between 800 and 1000°C. Figure 2.17 shows similar data for rupture time at several temperatures. Figure 2.18 shows a plot that relates the secondary creep rate to the applied stress at several temperatures. Figures 2.19 and 2.20 show correlations using the Larson Miller parameter to depict time for 1% creep strain and rupture as functions of test time and temperature.

Low-cycle fatigue, creep-fatigue, and crack-growth rate tests on Alloy 617 have been conducted by several researchers to establish the susceptibility of the alloy to cyclic loading and also to evaluate the role of surface interactions of coolant on the fatigue crack initiation and propagation (Strizak et al. 1982, Meurer et al. 1984, Hsu 1991). Figure 2.21 shows the fatigue behavior of Alloy 617 with several conventional materials at 538°C (Strizak et al. 1982).

Hastelloy X is a nickel-base superalloy with good oxidation resistance at temperatures up to ≈1200°C and moderately good strength properties at temperatures up to 870°C. It is essentially a single-phase austenitic alloy, which is a solid solution strengthened by additions of Cr, Mo, and W. Several studies have been conducted in the U.S. and in Japan to evaluate the tensile, creep rupture, low-cycle fatigue, creep fatigue properties, and fatigue crack growth of Hastelloy X, specifically for application in the helium environment of an HTGR (Lee 1984, Kurata et al. 1984, Nakanishi and Kawakami 1984, Tsuji and Kondo 1984, Bruch et al. 1984, Krompholz et al. 1984, Strizak et al. 1982).

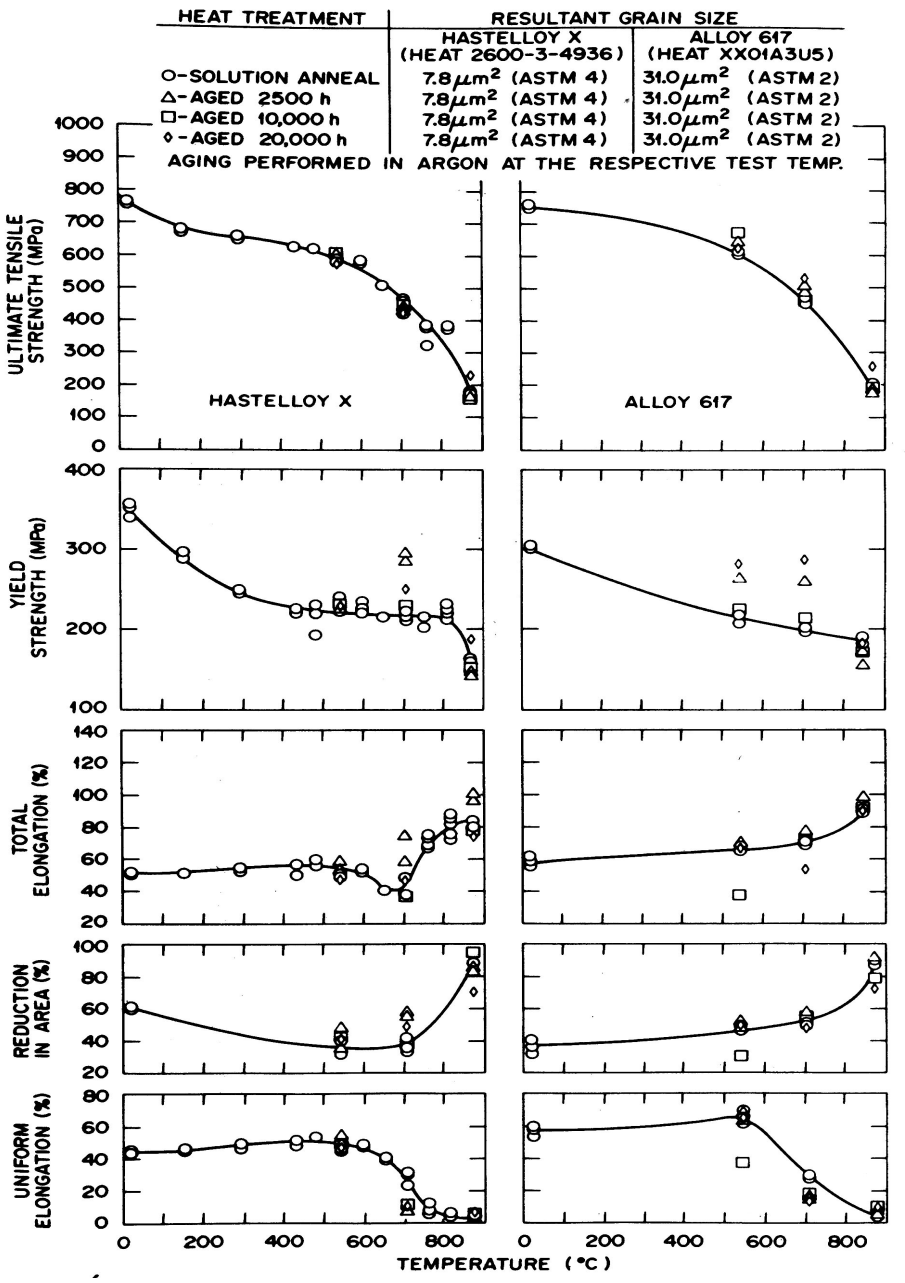

Figure 2.15 Tensile properties of Hastelloy X and Inconel 617 in both solution-annealed and aged conditions (Strizak et al. 1982).

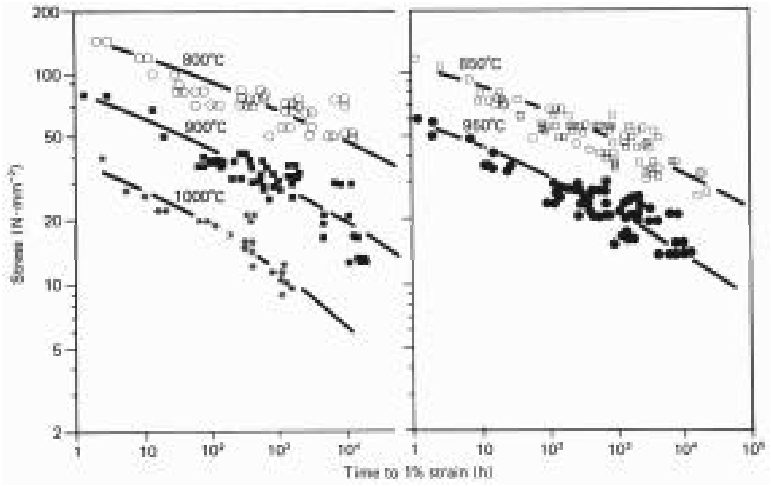

Figure 2.16 Applied stress versus time-to-1% strain from creep of Alloy 617 at several temperatures (Schubert et al. 1984).

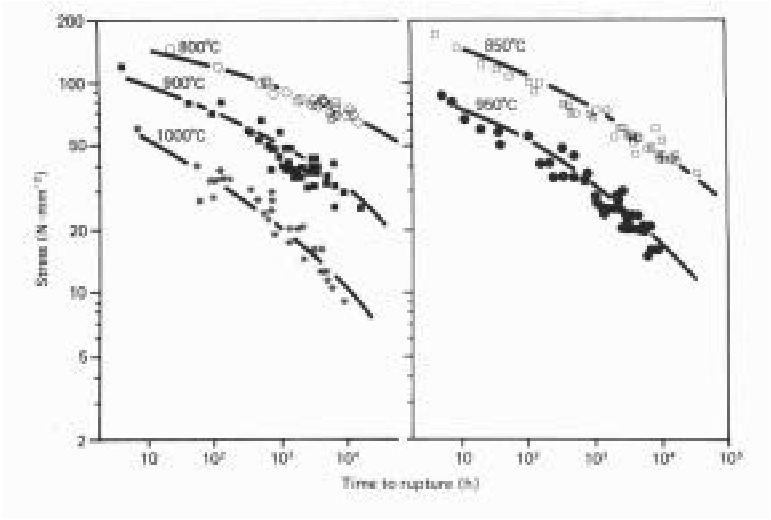

Figure 2.17 Applied stress versus time-to-rupture from creep of Alloy 617 at several temperatures (Schubert et al. 1984).

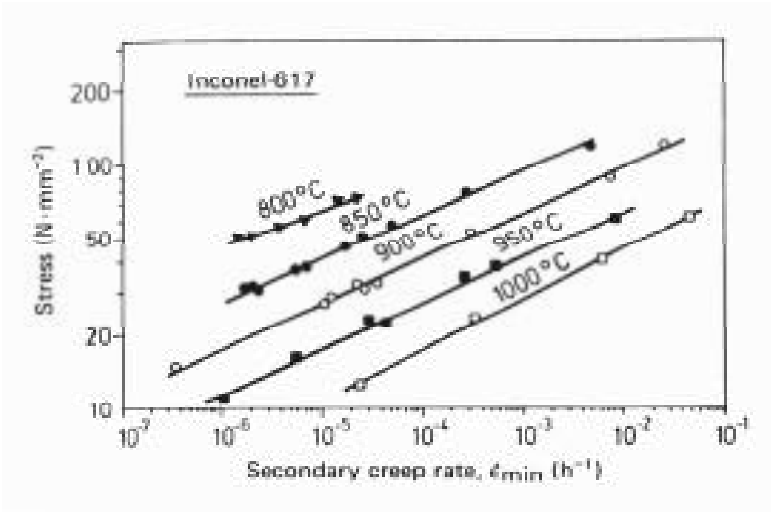

Figure 2.18 Applied stress versus secondary creep rate for Alloy 617 at several temperatures (Schubert et al. 1984).

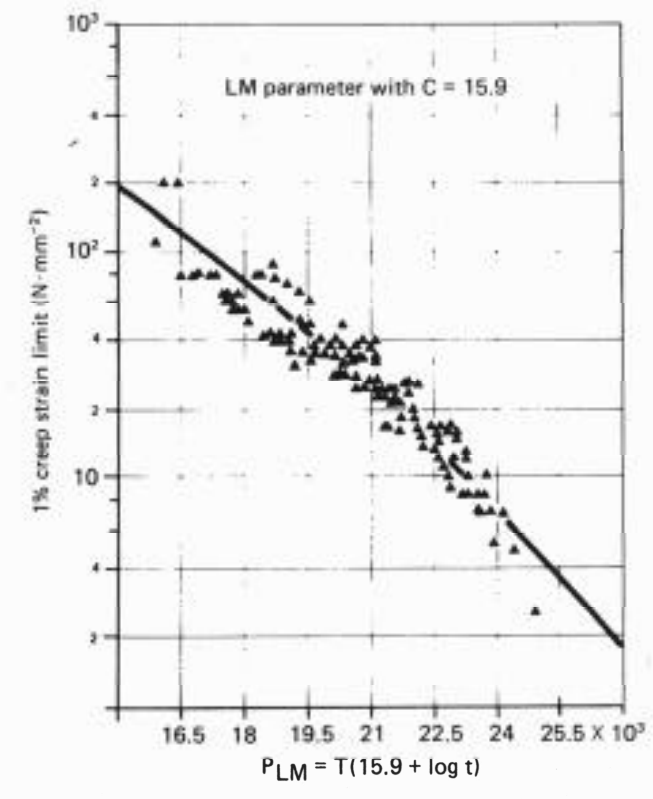

Figure 2.19 Larson-Miller parameter versus time-to-1% strain for Alloy 617 (Schubert et al. 1984).

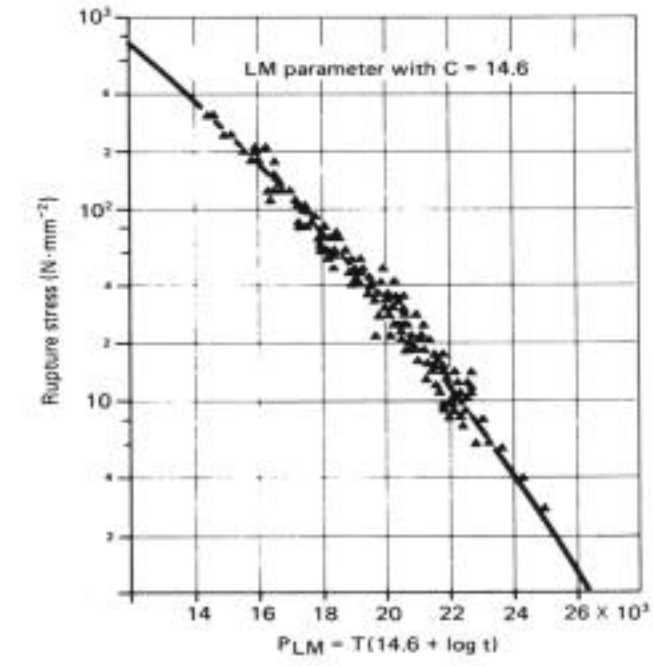

Figure 2.20 Larson-Miller parameter versus time-to-rupture for Alloy 617 (Schubert et al. 1984).

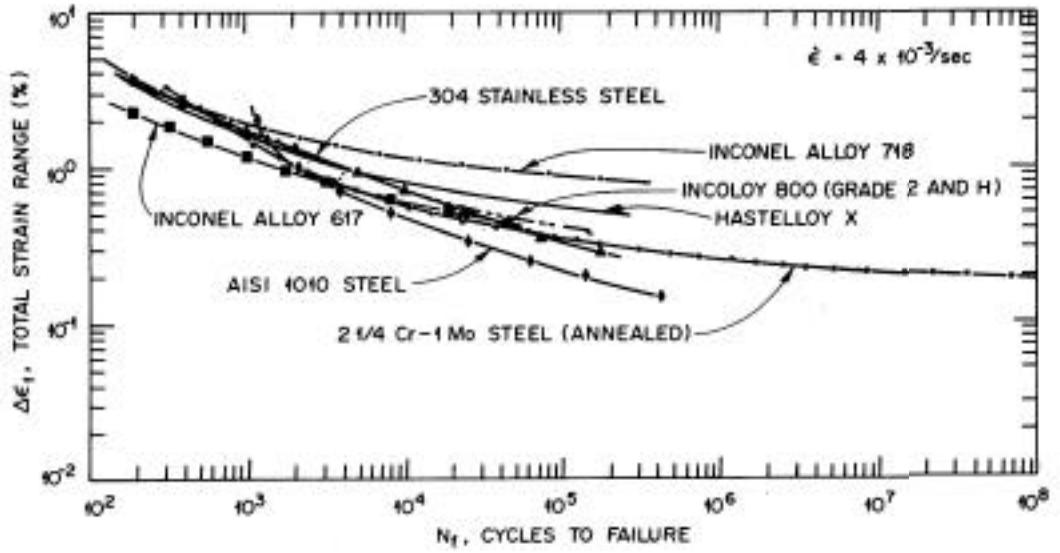

Figure 2.21 Comparison of fatigue behavior of Alloy 617 with several conventional materials at 538°C. Lines represent best fit of experimental data (Strizak et al. 1982).

Figure 2.22 shows the data on rupture time variation with applied stress for Hastelloy X at 760 and 871°C. Data generated for times up to 20,000 h showed that the rupture ductility for the alloy is fairly high in an air environment (Lee 1984). Figure 2.23 shows the variation in minimum creep rate as a function of applied stress for the alloy at 760 and 871°C. Figure 2.24 shows the low-cycle fatigue behavior of Hastelloy X at several temperatures in air (Strizak et al. 1982). Lines in the figure represent the best fit of experimental data.

Apart from Alloy 617 and Hastelloy X, several additional superalloys have been examined, albeit to a lesser extent, for elevated temperature application in HTGRs. These alloys include Nimonic-86, Hastelloy S, Manaurite-36X, and Inconel 519; available data on the mechanical properties for these alloys are given in several of the references cited above for Alloy 617 and Hastelloy X.

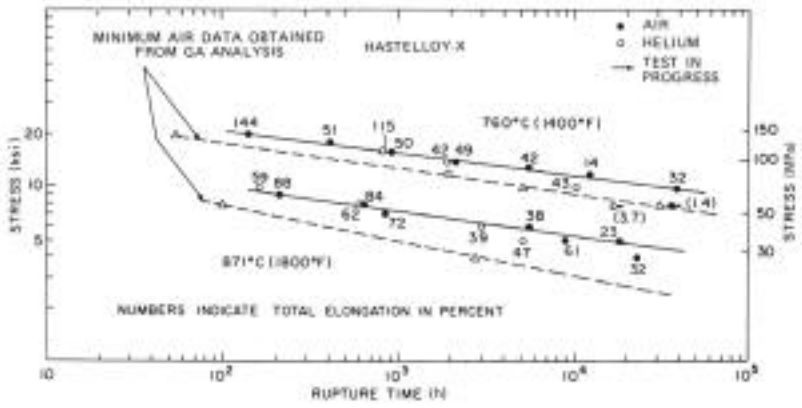

Figure 2.22 Applied stress versus rupture time for Hastelloy X at 760 and 871°C (Lee 1984).

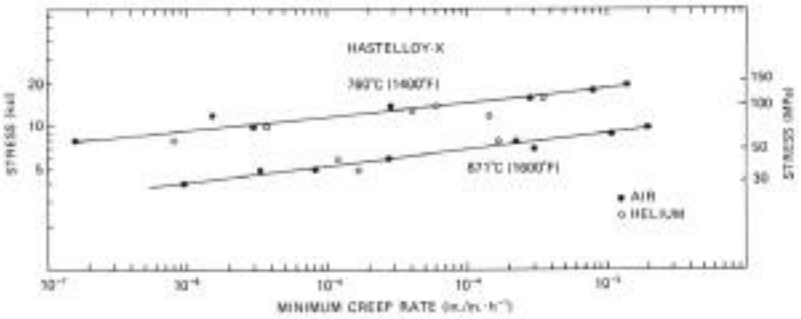

Figure 2.23 Applied stress versus minimum creep rate for Hastelloy X at 760 and 871°C (Lee 1984).

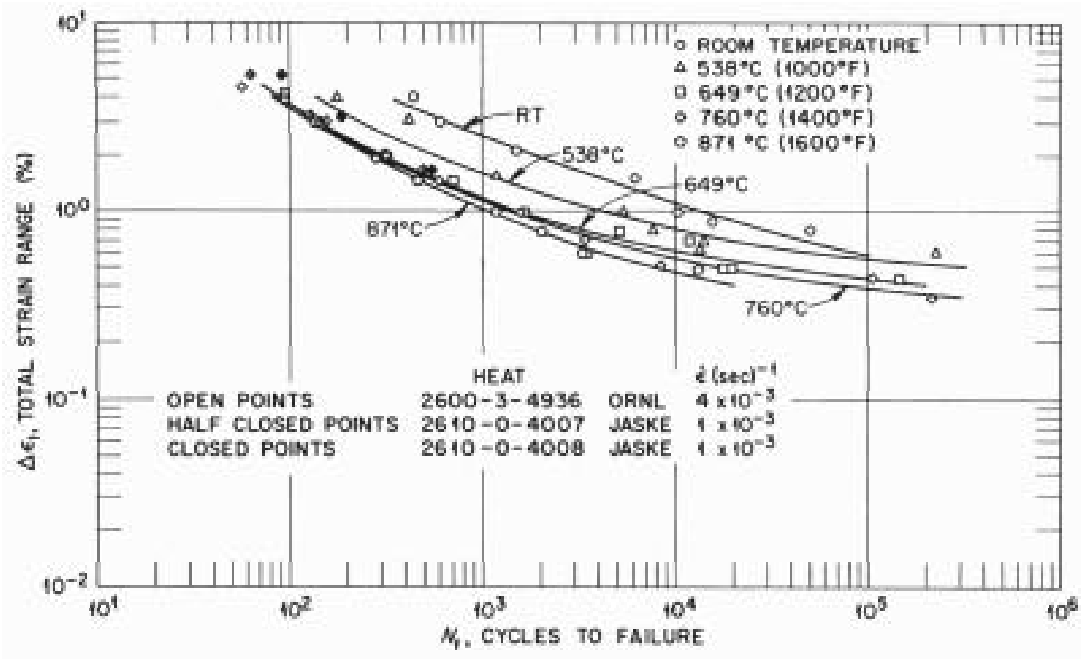

Figure 2.24 Low-cycle fatigue behavior of Hastelloy X at several temperatures in air. Lines represent best fit of experimental data (Strizak et al. 1982).

2.2 Power Conversion Materials

The GT-MHR module consists of a nuclear reactor as the source of heat and a power conversion system (PCS) (IAEA 2000, Courturier and Escaravage 2002). The PCS receives the thermal energy from the reactor system and converts it to usable electrical energy, with an overall efficiency of >45%. The PCS includes a turbomachine, precooler, intercooler, and connecting pipelines. The turbomachine consists of a turbocompressor, electrical generator, bearings, and seals. The turbocompressor includes the turbine and compressor sections.

The helium received by the PCS is expanded through the gas turbine that is coupled to the electrical generator. From the turbine exhaust, the helium flows through the hot side of the recuperator, transferring heat to helium returning to the reactor. The helium leaving the hot side of the recuperator is cooled before passing through the low-pressure compressor, intercooler, and high-pressure compressor. The helium then passes in the cold side of the recuperator, where it is heated for return to the reactor system.

The entire PCS assembly is installed in a vertical orientation and operates at a rotational speed of 3000 rpm. In the GT-MHR concept, a 12-stage turbine with high efficiency is proposed. With turbine inlet temperature of 850°C, blade and disk cooling are not considered as necessary in the design (Courturier and Escaravage 2002). It was reported that the materials for the turbine blades and disks should ensure a design life of 60,000 h, and the alloys selected for the blade and the disk should have minimum strength of 225 and 180 MPa, respectively, at 850°C (OKBM 1997).

2.2.1 Turbine Blade Alloys

Two classes of alloys, namely, nickel-base superalloys and molybdenum-based alloys, are being considered for blade application. The nickel-based superalloys include 713LC, M21, and MAR-M 004 (Courturier and Escaravage 2000).

Alloy 713LC is a cast nickel-base precipitation-hardened alloy that combines good creep rupture characteristics and excellent strength and ductility at room temperature. In addition, the alloy contains neither cobalt nor tantalum; these elements have been excluded for use in the primary circuit because of potential radioactive contamination. The alloy is reported to be well suited for the HTGR turbine blades, except for the first row of blades where cooling would be necessary to achieve the required lifetime (Kohler 1995). Alloy M21 is a low-chromium nickel-base cast alloy that combines precipitation hardening (Mo, Al, Nb) and solid-solution hardening (W). Alloy MAR-M 004 is a Hf-modified version of 713LC in which the Hf seems to improve the fracture toughness of the material.

Among the molybdenum-base alloys, Mo-TZM is a prime candidate that has been studied from the standpoint of fabrication, heat treatment, tensile, and creep rupture properties. An alloy with a composition of Mo-0.5 wt.% Ti-0.8 wt.% Zr has been produced by vacuum arc melting and by powder metallurgy (Jakobeit 1983).

2.2.2 Turbine Disk Alloys

The materials for the turbine disk application include Inconel 718, Udimet 720, MA 6000, A286, Waspaloy, and Inconel 706. The alloy Inconel 718 derives its high temperature strength by precipitation of gamma-prime [$Ni_3(Al,Ti)$] and gamma-double-prime (Ni_3Nb) phases. The time-temperature-precipitation plot of the alloy shows that both phases precipitate in the temperature range of ≈700 to 900°C and that the (Ni_3Nb) precipitates first while the $Ni_3(Al,Ti)$ precipitates over longer aging times (Brooks and Bridges 1988). An extensive database is available on the mechanical properties of Inconel 718 (Huntington Alloys 1978, Blatherwick and Cres 1966). The data show that at a turbine inlet temperature of 850°C, the alloy would require cooling to lower the temperature of the disks to ≈650°C to achieve the desired lifetime.

Alloy A-286 is a wrought iron-nickel γ'-strengthened superalloy that contains 2.1 wt.% Ti and 0.3 wt.% Al. The γ' phase $Ni_3(Ti,Al)$ in this alloy is metastable and is reported to transform from the strengthening cubic γ' to a weakening plate-like hexagonal eta phase on exposure at temperatures >650°C (Ross and Sims 1987). This limits the use of this alloy to a maximum temperature of 650°C. Alternatively, alloys containing cobalt (such as Udimet 700 and 720) generally possess high strength at elevated temperatures but need development for use as uncooled blades with the desired lifetime.

Alloy MA 6000, a nickel-base alloy produced by mechanical alloying, is an oxide-dispersion-strengthened superalloy with high strength and microstructural stability. The alloy combines solution strengthening by tungsten and molybdenum, precipitate strengthening by coherent γ' (Ni_3Al), and dispersion strengthening by yttria. Precipitate hardening enhances strength at intermediate temperatures, and the dispersion hardening improves the strength at temperatures >950°C. Creep properties of the alloy, evaluated in several studies, show that the alloy can be used in the uncooled condition in HTGR, but substantial additional effort is needed for producing large ingots with homogeneous composition by hot isostatic pressing or hot extrusion and for acquiring long-term mechanical property data (Howson et al. 1980, Been 1987).

3 Helium Coolant Effects

The focus of this Section is to examine the influence of helium coolant on the chemical compatibility of structural materials that are planned for use in HTGRs. Helium, because of its chemical inertness and attractive thermal properties, is used as a primary coolant in HTGRs. However, the primary coolant in an operating HTGR is expected to be contaminated by small amounts of gaseous impurities such as H_2, H_2O, CH_4, CO, CO_2, and O_2 from a variety of sources, such as reactions of ingressed water and oil with core graphite, and outgassing of reactor materials. These impurities are projected to be in ppm levels in the helium coolant, but the upper bound would strongly depend on the level of purification used for the helium supply and the leak tightness of the reactor system. Corrosion of structural alloys by these gaseous impurities at elevated temperatures can be significant. Past studies have shown that the corrosion of heat resistant materials such as austenitic stainless steels, Alloy 800H and 617 may involve oxidation, carburization, and decarburization depending on the exposure temperature, carbon activity in the gas phase, and the alloy composition. Further, the corrosion process is dynamic in the sense that it is dictated by the exposure time, gas chemistry variations, integrity of the corrosion product scales, and presence of particulates in the gas phase.

3.1 Coolant Chemistry

The helium coolant in an operating HTGR makes a complete circuit from the graphite core to the heat exchangers or gas turbines and back to the core in several seconds. It is reported that the gas components in the coolant, via reaction with the graphite in the core and, to a limited extent, with themselves, will reach a steady state under this dynamic flow condition and may approach an equilibrium state with respect to the core (Johnson and Lai 1981). Equilibrium between the surfaces of metallic components and the gaseous impurities in the primary coolant helium is not expected to occur under these very fast flow conditions. Therefore, the carbon activity and oxygen partial pressure in the helium coolant, under such nonequilibrium conditions, will be determined by individual reactions that predominate in the gas mixture.

Although the gaseous impurities in a primary coolant environment may not be in equilibrium with themselves or with surfaces of metallic components, driving forces will exist for gas-metal interactions to occur. The extent to which these interactions will occur will be kinetic controlled, dictated by time, temperature, alloy chemistry, and surface condition of the alloy. In such nonequilibrium conditions, potentials for gas-metal corrosion reactions may be determined through equilibrium thermodynamics by considering each individual chemical reaction that is possible between the metal and individual gaseous impurities.

From the structural materials standpoint, we are interested in reactions that can affect the corrosion loss and/or influence the mechanical integrity; reactions that can lead to processes such as oxidation, carburization, and decarburization are of interest. Carburization and decarburization processes are determined by the carbon activity in the gas mixture relative to that in the exposed metal surface. Similarly, the oxidation process is determined by the oxygen partial pressure in the environment relative to the stability of oxides of the constitutive elements that are present on the exposed metal surface.

Carbon activity in the gas phase may be determined by any of the reactions listed below:

$$CO + H_2 = C + H_2O, \quad (2)$$

$$2CO = C + CO_2, \quad (3)$$

$$CH_4 = C + 2H_2, \quad (4)$$

$$CH_4 + CO = 2C + H_2O + H_2, \quad (5)$$

$$CO = C + 1/2\ O_2, \quad (6)$$

The carbon activity in the gas phase for each of the five reactions may be calculated from its equilibrium constant (K) via the partial pressure (p) of each component:

$$a_C = K_1\ (p_{CO} \cdot p_{H_2})\ /\ p_{H_2O} \text{ for Reaction (2)}, \quad (7)$$

$$a_C = K_2\ (p_{CO})^2 /\ p_{CO_2} \text{ for Reaction (3)}, \quad (8)$$

$$a_C = K_3\ p_{CH_4}\ /\ (p_{H_2})^2 \text{ for Reaction (4)}, \quad (9)$$

$$a_C = (K_4)^{1/2} \cdot (p_{CH_4} \cdot p_{CO}\ /\ p_{H_2O} \cdot p_{H_2})^{1/2} \text{ for Reaction (5)}, \quad (10)$$

$$a_C = K_5\ p_{CO}\ /\ (p_{O_2})^{1/2} \text{ for Reaction (6)}. \quad (11)$$

In the absence of thermodynamic equilibrium between all the species in the gas phase, the carbon activity in the environment will be established by any of the reactions listed above, and the dominant reaction is probably the one that gives the highest carbon activity.

The oxygen partial pressure in the helium environment will be determined by the following reactions, in addition to Reaction (6):

$$H_2O = 1/2O_2 + H_2, \quad (12)$$

$$CO_2 = 1/2O_2 + CO. \quad (13)$$

The oxygen partial pressure established by these reactions can be calculated as follows:

$$pO_2 = (K_5 \cdot p_{CO} /\ a_C)^2 \text{ for Reaction (6)}, \quad (14)$$

$$pO_2 = (K_6 \cdot p_{H_2O} /\ p_{H_2})^2 \text{ for Reaction (12)}, \quad (15)$$

$$pO_2 = (K_7 \cdot p_{CO_2} /\ p_{CO})^2 \text{ for Reaction (13)}. \quad (16)$$

3.1.1 Equilibrium versus Nonequilibrium Gas Chemistry

When equilibrium prevails between various gas species in a multicomponent gas mixture, the carbon activity and oxygen partial pressure in the gas environment are determined from the minimization of free energy for the gas mixture as a whole at a given temperature. This

means that all the species in the gas mixture are in thermodynamic equilibrium, and that the kinetics of reactions does not play a role in determining the values. Therefore, the calculated carbon activity and oxygen partial pressure are unique for a given temperature and are independent of the reactions given above. Under these conditions, the interactions of the gas species with material surfaces can be analyzed using equilibrium thermodynamics on gas-metal interactions to establish the surface reaction products as a function of gas chemistry, temperature, alloy chemistry, and exposure time.

On the contrary, if the gas species in the multicomponent gas mixture are not in equilibrium, then one or more of the reactions discussed above will influence the actual gas composition (at a given temperature). Furthermore, the composition can change with time influenced by the kinetics of these reactions. Therefore, determining which of the reactions dictates the carbon activity and oxygen partial pressure is difficult, if not impossible, and understanding the variation of these parameters with time is even more complex. In an HTGR environment, the gas phase composition is probably determined by the level of impurities in the helium at the reactor inlet, which is modified by reactions with graphite in the core at elevated temperatures. Therefore, one can establish an anticipated envelope for the gas chemistry, based on a mass balance and reaction equilibrium at the core temperatures. The gas chemistry thus calculated may be modified along the primary loop by the reactions discussed above, but the variation may be small, since the flow rate of helium is high and the residence time is relatively small.

3.1.2 Effect of System Pressure

System pressure can significantly affect on the calculations of carbon activity and oxygen partial pressure, depending on which of the reactions (discussed above) predominantly controls the process. In experiments that are conducted at a total pressure of 1 atm, the partial pressures and concentrations of the species are essentially the same. On the contrary, in a high-pressure environment, the partial pressure of a species is the product of concentration of that species and the system pressure. As a result, for a given gas composition, the carbon activity calculated using different reactions discussed above is affected differently by the system pressure. For example, carbon activity calculated by Eqs. (7) and (8) increases in proportion to an increase in system pressure. Carbon activity calculated by Eq. (9) decreases with an increase in system pressure while that calculated by Eq. (10) is unaffected by system pressure. Carbon activity calculated by Eq. (11) increases with the square root of system pressure.

For a given oxygen concentration, the oxygen partial pressure is calculated by Eqs. (14), (15), or (16). The values calculated by Eqs. (15) and (16) are unaffected by variations in system pressure, but the values calculated by Eq. (14) increase directly with an increase in system pressure. The effect of system pressure on gas-metal reactions is not adequately addressed in the literature.

3.2 Effect of Impurities on Corrosion

The basis for the selection of impurity concentration range is the HTGR systems that are designed using steam cycles for generating electricity or process heat. The thinking on the anticipated levels of impurities went as follows (Graham et al. 1981).

The helium entering the core has a certain amount of oxygen and H_2O. First, the hot graphite core removes virtually all free oxygen to form CO, but the slower kinetics of the reaction of the graphite core with H_2O leads to only partial reaction, and hence the helium contains traces of H_2O together with H_2 and CO produced by the reaction of some of the H_2O with the core. Any CO_2 which is present from degassing of the graphite reflectors is also largely converted to CO by reaction with the hot core. The level of H_2 is increased relative to that expected from the reaction of H_2O with the graphite by proton inleakage from boilers or process reaction, but some H_2 also reacts with the cooler parts of the core via a radiolytic reaction to produce CH_4. Oil inleakage can also lead to CH_4 production. However, the CH_4 tends to be removed by thermal cracking in the hotter parts of the core. The residual amount in the helium depends on the actual peak core temperature, higher temperatures leading to lower CH_4 levels. Therefore, the main impurities in the primary circuit helium were identified as H_2, H_2O, CO, CH_4, and N_2.

The actual levels of impurities in a given system depend on the detailed design and construction features such as the purification ratio, the type of gas circulators, and the choice of graphite/carbon used. The ranges expected in steam- and gas-turbine-based HTGRs, under normal operating conditions, are estimated as shown in Table 3.1 (Graham et al. 1981).

The levels of impurities in the helium coolant will be different for the steam-generating and direct-cycle gas-turbine HTGR systems. One of the major differences lies in the oxygen potential (or oxygen partial pressure) of the environment. In the case of the steam-cycle system where continuous ingress of low levels of water and steam into the primary coolant is possible, the environment is expected to have a relatively higher oxygen potential (i.e., high ratios of H_2O to H_2). In the gas-turbine-based system, it is anticipated that the helium coolant will be much "drier" (i.e., low ratios of H_2O to H_2) owing to the lack of potential sources of continuous water and steam ingress. With the understanding that the impurity types and concentrations differ between the steam-based and gas-turbine-based systems, we will next examine the available information on materials performance in such environments.

3.2.1 Reaction in Single-Oxidant Environments

Considerable research on the causes, effects, and prevention of different types of corrosion has been underway for many years. However, when one studies reaction kinetics

Table 3.1 Range of impurity levels (in Pa) expected in HTGR helium coolants

	Range of partial pressure (Pa)	
Impurity	Steam cycle	Gas turbine cycle
H_2	20	50
H_2O	1	0.05
CO	1	5
CH_4	2	5
CO_2	<0.1	<0.1
N_2	1.5	1.5
O_2	<<<0.1	<<<0.1

that involves only one reaction equilibrium, such as H_2O/H_2 or CO_2/CO for oxidation or CH_4/H_2 for carburization, the reaction potential of the participating species can be established by the standard free energy of formation for the reaction. For an oxidation reaction of a pure metal M, such as

$$M + 1/2\ O_2 = MO, \tag{17}$$

the oxygen partial pressure (pO_2) for the M/MO_2 equilibrium is given by

$$pO_2 \text{ at } M/MO_2 \text{ phase boundary} = \exp(\Delta G^\circ/RT), \tag{18}$$

where ΔG° is the free energy change for the M/MO_2 equilibrium at temperature T. In binary and ternary alloys, the activities of the reactive element (a_M) and the oxide (a_{MO_2}) should also be considered. In such cases, Eq. (18) becomes

$$pO_2 \text{ at } M/MO_2 \text{ phase boundary} = a_{MO_2} / a_M \exp(\Delta G^\circ/RT). \tag{19}$$

In general, element activity in an alloy is given by

$$a_M = \gamma_M \cdot X_M, \tag{20}$$

where γ_M and X_M are the activity coefficient and mole fraction of M in the alloy, respectively. If γ_M is not known, ideal behavior is assumed, and γ_M is assigned a value of unity.

Under similar single-oxidant conditions, the oxidation or carburization of a metal can be established by the standard free energy of formation of the metal oxide or carbide. Plots of standard free energy of formation versus temperature for compounds such as oxides and carbides are given in the literature and serve as a guide in establishing the relative stability of the corrosion-product layers with respect to both the partial pressure of the reactive species in the exposure environment and the alloy composition.

Figures 3.1 and 3.2 show the thermodynamic stability of several oxide and carbide phases that form by reaction between oxygen or carbon and the constituents of various structural materials such as heat-resistant alloys, superalloys, and refractory metals. As a result, in classical studies on materials exposed to single oxidants, the central theme is to understand the kinetic aspects of continuous scale development and the mechanisms of scale growth as a function of variables such as temperature, time, and reactant activity in the exposure environment. An enormous literature exists on nucleation and growth of corrosion-product scales for a wide range of materials exposed to several single-oxidant environments. In addition, the effort has concentrated on modifying alloy compositions to (a) form slower growing scales (for example, alumina, chromia, or silica scales instead of iron oxides, NiO, or CoO in heat-resistant iron-, nickel-, and cobalt-base alloys), (b) reduce corrosion rates (smaller parabolic rate constants), (c) improve adhesion of scales to substrates (by additions of reactive elements such as Y, Ce, and La), especially under thermal cycling conditions, and (d) provide surface enrichment of structural alloys with elements (such as Cr, Al, and Si on low- and intermediate-chromium steels, and austenitic alloys) that form slow-growing oxide scales.

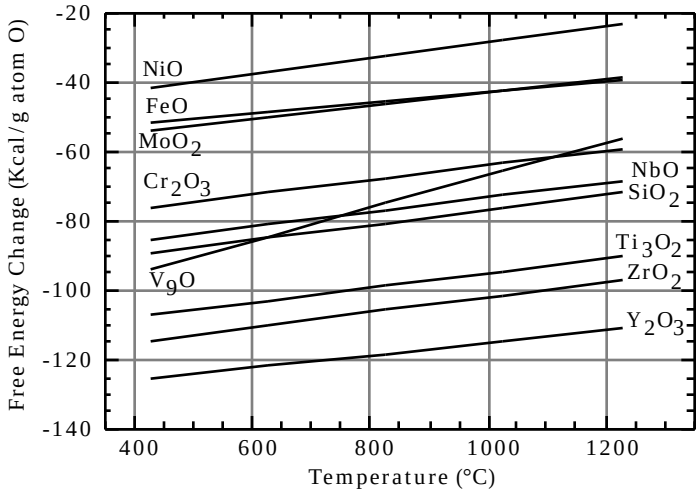

Figure 3.1 Thermodynamic stability of various oxides as a function of temperature.

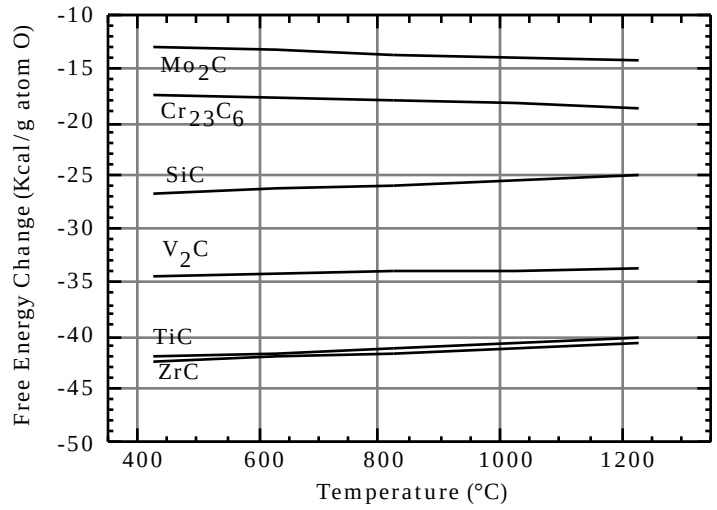

Figure 3.2 Thermodynamic stability of various carbides as a function of temperature.

3.2.2 Reaction in Bioxidant Environments

When materials are exposed to multicomponent gas environments or mixed oxidants, the oxidation and carburization processes mentioned above can occur simultaneously. Furthermore, the second reactant may either modify or degrade the corrosion-product layers that form by reaction of the first reactant and the substrate elements. In these situations, reactions will occur not only at the gas/scale interface, but also within the scales that develop on the surface and in the base metal beneath the reaction products. As a result, the development of suitable and meaningful thermodynamic and kinetic frameworks for both nucleation and growth of scale layers on materials exposed to mixed-oxidant atmospheres is quite complex.

When studying reactions between metallic alloys and complex gas environments, the chemical activities of several reactive species in the gas phase must be considered simultaneously, and these activities are generally established by gas-phase equilibria, especially at elevated temperatures. In binary and ternary gas mixtures, the chemical potentials of the reactive species can be readily established, as a function of temperature, from

the room–temperature gas composition and free energy data for reactions. For a gas system that consists of CO, CO_2, H_2, H_2O, CH_4, and N_2, several gas equilibria have been used to formulate a set of nonlinear algebraic equations (Natesan 1976, Chopra and Natesan 1977). One can use iterative procedures to determine the gas compositions at elevated temperatures that yield minimum free energy for the system and satisfy the conservation of different reactive elements (i.e., C, H, O, and N) and the total pressure of the gas mixture. Results of such analyses have been used to establish the elevated-temperature gas compositions, the partial pressures of oxygen and nitrogen, and the carbon activity in the gas mixture. Analyses of gas/metal interactions in mixed-gas atmospheres assume that equilibria among various molecular gas species prevail, and chemical activities are calculated by using the above approach or some similar method. However, under nonequilibrium conditions, the oxygen partial pressure and carbon activity will be determined by any of the possible reactions, as was discussed in Section 3.1.

We next address the thermodynamic aspects of metal corrosion in a bioxidant situation, such as an oxygen/carbon environment. The following surface reactions are possible on a divalent metal A:

$$A + 1/2\ O_2 = AO, \tag{21}$$

$$A + C = AC, \tag{22}$$

where AO and AC are the oxide and carbide reaction products, respectively. Under equilibrium conditions, the partial pressures of oxygen and activity of carbon are defined by the relations

$$(a_O)_{eq} = pO_2^{1/2} = \exp(\Delta G_{AO}/RT), \tag{23}$$

$$(a_C)_{eq} = \exp(\Delta G_{AC}/RT), \tag{24}$$

where ΔG_{AO} and ΔG_{AC} are the standard free energies of formation of the oxide and carbide, respectively, at temperature T. From Eqs. (23) and (24), one should be able to deduce the conditions for oxidation or carburization; however, a further reaction must be considered, namely

$$AC + 1/2\ O_2 = AO + C, \tag{25}$$

with the equilibrium condition

$$(a_C/a_O)_{eq} = \exp[(\Delta G_{AC} - \Delta G_{AO})/RT]\ a_{AC}/a_{AO}. \tag{26}$$

If we assume unit activity for the phases AC and AO, Eq. (26) is reduced to

$$(a_C/a_O)_{eq} = \exp[(\Delta G_{AC} - \Delta G_{AO})/RT]. \tag{27}$$

Examination of Eqs. (23), (24), and (27) permits the identification of various situations that limit the type of surface corrosion products that can be formed, as follows:

$$\text{(i)} \quad \text{if } (a_O)_{gas} > (a_O)_{eq} \text{ and } (a_C)_{gas} < (a_C)_{eq}, \tag{28}$$

then AO is the only stable surface phase;

$$\text{(ii)} \quad \text{if } (a_O)_{gas} < (a_O)_{eq} \text{ and } (a_C)_{gas} > (a_C)_{eq}, \tag{29}$$

then AC is the only stable surface phase; and

$$\text{(iii)} \quad \text{if } (a_O)_{gas} > (a_O)_{eq} \text{ and } (a_C)_{gas} > (a_C)_{eq}, \tag{30}$$

then both AO and AC should be stable and form as surface products. However, reference to Eq. (25) indicates that only one phase will form, depending on which of the following conditions prevails:

$$\text{(a)} \quad (a_C / a_O)_{gas} > (a_C / a_O)_{eq}, \tag{31}$$

$$\text{(b)} \quad (a_C / a_O)_{gas} < (a_C / a_O)_{eq}. \tag{32}$$

Condition (a) will cause Eq. (25) to proceed to the left, and AC will be the stable phase where the metal is in contact with the gas phase. In condition (b), AO will be the stable phase, and Eq. (25) will proceed to the right.

A convenient way of representing the possible corrosion products as a function of gas chemistry is to construct thermochemical diagrams that depict the stability ranges of various condensed phases as functions of the thermodynamic activities of the two components of the reactive gas. Figure 3.3 shows a thermochemical stability diagram for the Cr–C–O system developed for a temperature of 982°C. In the construction of this diagram, the thermodynamic activities of the metal and corrosion–product phases are assigned a value of unity. In multicomponent alloys, the activities of constituent elements will be less than unity and should be accounted for in the analysis. Further, in gas/solid reactions that involve multicomponent alloys, a more complex corrosion product (i.e., more complex than a binary compound) can result that would decrease the thermodynamic activities of the specific phase in the mixture.

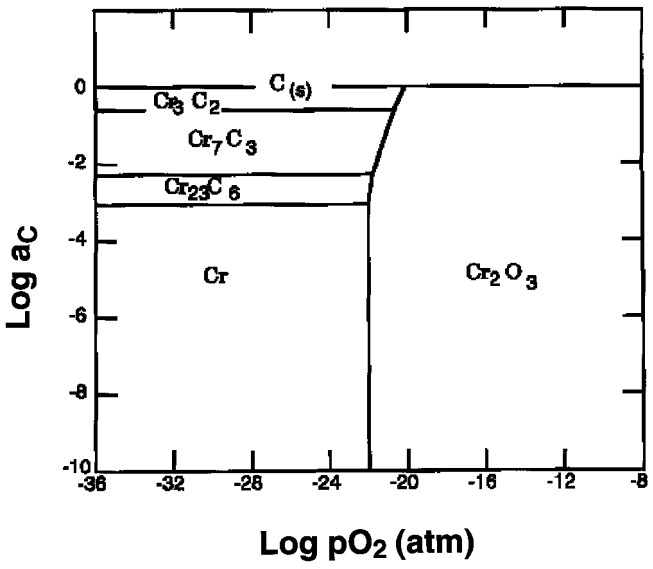

Figure 3.3 Thermochemical diagram for Cr-C-O system at 982°C, indicating the stability region of various phases.

3.2.3 Corrosion Performance Data

A significant body of corrosion information has been developed on several candidate alloys exposed to helium environments with a narrow range of impurity concentrations (Brenner and Nilsen 1978, Graham et al. 1981, Johnson and Lai, 1981, Kondo 1981, McKee and Frank 1981, Bates 1984, Cappellaere et al. 1984, Kondo 1984, Huchtemann 1989, and Graham 1990). The selected gas compositions were based predominantly on steam-cycle HTGRs, which were envisioned during the 1970s and 1980s. A listing of gas compositions used in several of the investigations is given in Table 3.2. Even though several studies have been conducted to evaluate the corrosion performance of structural materials in helium that contained different concentrations (in a somewhat narrow range) of impurities such as H_2, H_2O, CH_4, CO, and CO_2, none of the studies was conducted with a systematic variation in gas composition to evaluate its influence on the scaling and its protective capacity at elevated temperatures. Figure 3.4 shows examples of scale morphologies that have been observed on Alloy 800H, Nimonic 86, and Alloy 617. There are variations in scaling depending on alloy chemistry. Scaing can also be influenced by gas chemistry in the exposure environment and temperature.

Johnson and Lai (1981) examined the carburization behavior of Alloys 800H and 617 and Hastelloy X in helium containing various amounts of H_2, H_2O, CH_4, CO, and CO_2, in a temperature range of 649 to 1000°C for exposure times up to 10,000 h. Four different helium environments, identified as A, B, C, and D (see Table 3.2), were used in the experiments. Environments A and B were characteristic of high-oxygen potential, whereas environments C and D were characteristic of low-oxygen potential. Thermodynamic calculations indicated that all four environments were reducing to iron oxides (and to thermodynamically less stable oxides of nickel, molybdenum, cobalt, etc.) and oxidizing to chromium and to elements more reactive than chromium (manganese, silicon, titanium, aluminum, etc.). Figure 3.5 shows the equilibrium partial pressure for several oxides as a function of reciprocal temperature, along with the calculated oxygen partial pressures, for environments A through D based on Reaction (12). Several conclusions were reported based on the results from the study.

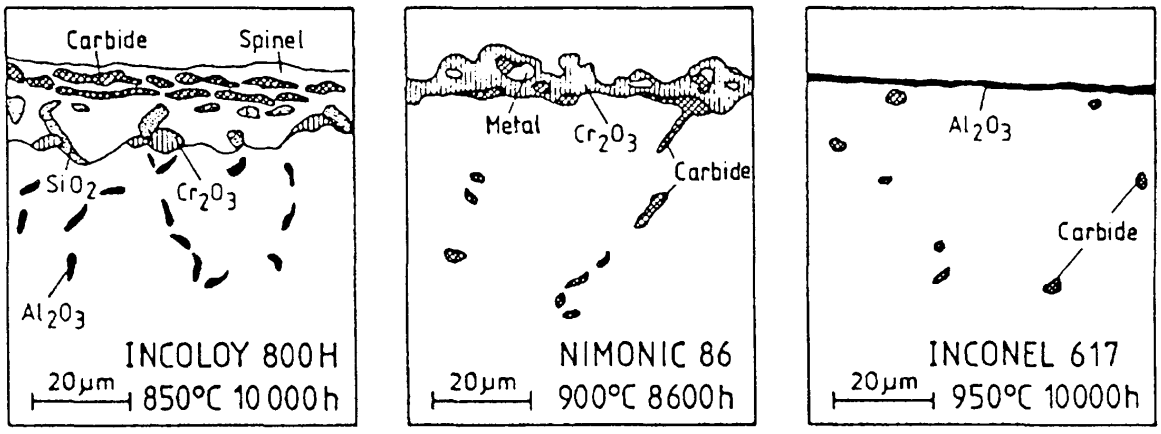

Figure 3.4 Different surface layers observed on high temperature alloys exposed to helium in high temperature reactor (Schubert 1984)

Table 3.2 Gas chemistries used in various investigations

Gas Identification	Gas composition (in Pa)						Reference
	H_2	CO	CH_4	CO_2	H_2O	N_2	
A	150	45	5	<0.05	5	-	Johnson and Lai 1981
B	20	10	2	0.5	5	-	Johnson and Lai 1981
C	50	5	5	<0.05	<0.05	-	Johnson and Lai 1981
D	50	5	5	<0.05	0.15	-	Johnson and Lai 1981, Brenner and Nilsen 1978
HTR	50	5	2	-	0.1	-	Graham et al. 1981
Decarb.	50	0.5	0.5	-	0.1	-	Graham 1990
Carb.	50	0.15	0.2	-	0.01	-	Graham 1990
JAERI-B	20	10	0.5	0.2	0.1	<0.5	Kondo 1981
ERANS#2	30	10	0.4	0.1	0.3	<0.5	Kondo 1981
PNP	50	2	2	0.1	<0.2	0.5	Kondo 1981, Quadakkers and Schuster 1984, Bates 1984
GE	40	4	2	0.02	0.2	0.6	McKee and Frank 1981
Lab I	150	45	5	-	5	-	Cappellaere et al. 1984
AIDA	150	45	5	-	5	-	Cappellaere et al. 1984
Lab II	50	1.5	2	-	0.15	0.5	Huchtemann 1989

ERANS: Engineering Research Association of Nuclear Steelmaking, Japan.
JAERI: Japanese Atomic Energy Research Institute.
HTR: High Temperature Reactor.
PNP: Prototype Nuclear Process.
GE: General Electric Company.
Lab I and Lab II: Environments in laboratory tests.

- Carburization was observed in all four environments. For all three alloys, carburization kinetics in the low-oxygen-potential environments (C and D) were significantly higher (approximately one order of magnitude) at elevated temperatures than those in the high-oxygen-potential environments (A and B) for all three alloys. The enhanced carburization was attributed to kinetic effects in low-oxygen-potential environments rather than the variation in gas chemistry.

- The scale formed on the metal surface in the high-oxygen-potential environments consisted of oxides of manganese and/or chromium, while the scale formed in the low-oxygen-potential environments consisted of Mn- and/or Cr-rich oxides and Cr-rich carbides.

- Controlling the oxygen potential of the service environment can be an effective means of reducing carburization of austenitic alloys. The effect of increasing the oxygen potential on the corrosion rates of HTGR core graphite must be considered in evaluating the practical application of this approach.

Graham et al. (1981) examined Alloy 617 and Nimonic 86 in a helium environment that was considered as a standard gas (see Table 3.2) for helium-cooled process heat systems by

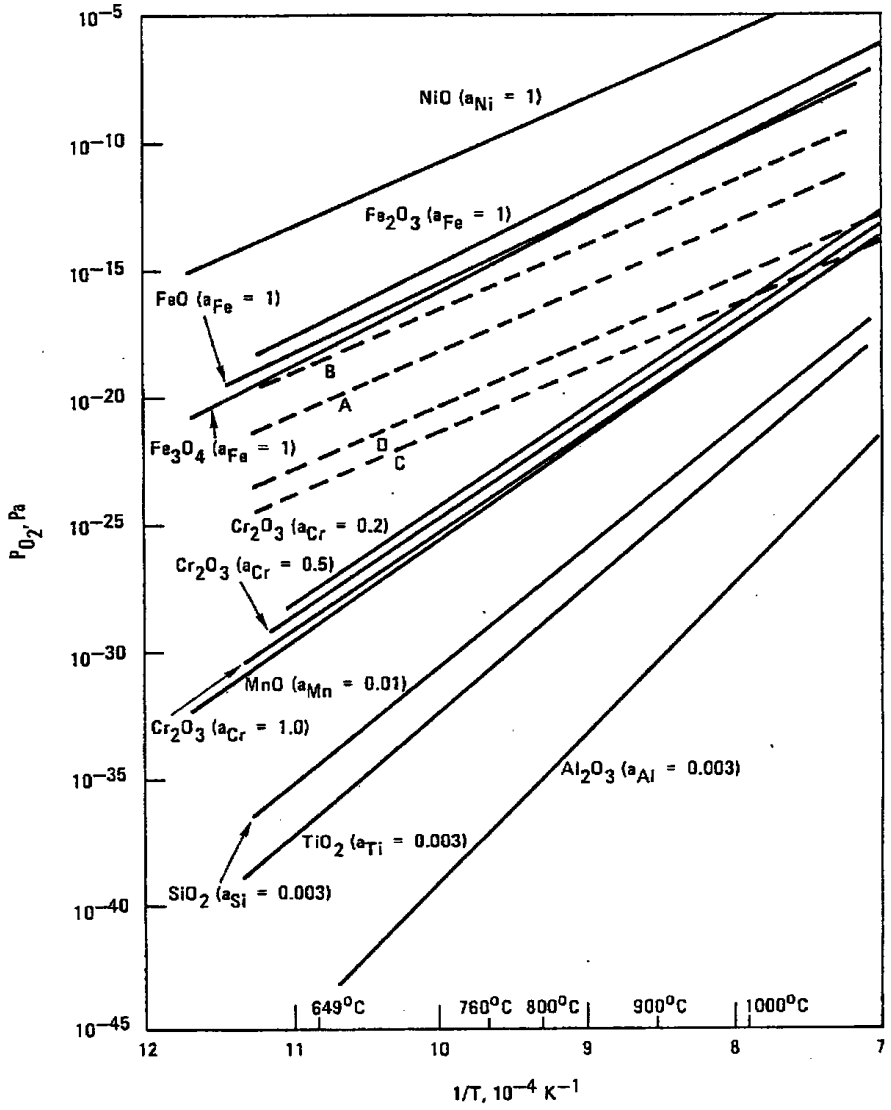

Figure 3.5 Equilibrium partial pressure for several oxides as a function of reciprocal temperature, along with calculated oxygen partial pressures, for environments A through D based on Reaction (12). Data from Johnson and Lai 1981.

exposing the alloys at temperatures between 800 and 1000°C for times up to 10,000 h. They related the degree of depletion or production of impurities caused by the gas/metal reactions that occur at the metal surface by a parameter relating the surface area of the specimen and volumetric flow of helium. The study reported several conclusions, as follows:

- Both the alloys developed thin, adherent, chromium-rich oxide scales. These scales gave excellent resistance to carburization, although scale variations occurred due to the influence of minor alloying elements such as titanium, aluminum, and manganese.

- The influence of variations in gas chemistry showed that if the CH_4/H_2O ratio is unfavorable, enhanced carburization resulted, and if the CO/H_2O ratio is unfavorable, decarburization was noted.

In a further study, Graham (1990) evaluated the long-term performance of Alloys 800H and 617 at temperatures between 400 and 1000°C from the standpoint of decarburization, carbon deposition/carburization, internal oxidation of the substrate, and spalling of the surface scales. Two different gas chemistries were used, identified as "Decarb" and "Carb" in Table 3.2. Several conclusions were reported from this study:

- Below ≈475°C corrosion is minimal, and the high-chromium alloys developed thin chromia scales. At temperatures up to 900°C, the high-chromium alloys exhibited thin chromia scales along with internal oxidation of aluminum and precipitate-free zones. Carburization effects are enhanced if the scale is porous or if it spalls. Above 900°C rapid decarburization or carburization occurred, depending on the gas chemistry.

- The onset of rapid carburization or decarburization occurred above a critical temperature that is dependent on the alloy composition and the CO partial pressure in the environment. It was postulated that at this critical temperature CO becomes relatively more stable than the metal oxide and metal carbide. Above the critical temperature, the H_2 in the environment reduces the chromia scale, and the released H_2O reacts with carbon in the alloy to form CO. Graham (1990) termed this mechanism as "gas catalyzed" reaction, whereas Brenner (1982) called it a "microclimate reaction." Brenner concluded that a "low" CH_4/H_2O ratio (i.e., excess H_2O) stabilized the Cr-based surface oxide and led to decarburization, whereas a "high" CH_4/H_2 ratio (i.e., excess CH_4) led to Cr-based surface carbide and continuous carburization.

Kondo (1981) evaluated the corrosion performance of Hastelloy X and XR in two gas mixtures (see Table 3.2) and concluded that Hastelloy X suffered from intergranular attack and internal oxidation. The modified alloy XR did not show appreciable susceptibility to such an attack, and it formed a continuous oxide film up to 1000°C in both environments. The kinetics of Cr depletion followed a parabolic rate law, based on exposures up to 6,000 h at 1000°C. The enhanced resistance of Hastelloy XR was attributed to formation of a double layer that consisted of an outer layer of $MnCr_2O_4$ and an inner layer of Cr_2O_3. Kondo also suggested that it is essential to maintain the ratio of the reacting metal surface to the volumetric flow rate of helium-containing impurities during experimentation, thereby minimizing the change(s) in gas chemistry during long exposure periods.

Bates (1984) established the long-term corrosion behavior of Alloys 800H and 617, Nimonic 86, and Hastelloy X for the primary circuit in the prototype nuclear process (PNP) reactor. Exposures were conducted in the temperature range of 700 to 900°C for times up to 10,000 h. In PNP helium chemistry (see Table 3.2), Nimonic 86 exhibited resistance to carburization at temperatures of 700 to 900°C, and this behavior was attributed to formation of defect-free chromia scales. Alloys 800H and 617 and Hastelloy X also showed good carburization resistance, but a slow increase in carbon level with a parabolic kinetics. This behavior was attributed to interference (in the formation of chromia scales) from other oxide-forming elements in the alloys. Complete resistance to spalling of the scales was reported in all

alloys, except Alloy 800H. The cause for severe spalling in Alloy 800H was attributed to the presence of 0.5 wt.% Si in the alloy. The good carburization resistance observed in the alloys was lost or severely reduced when water levels in the gas dropped below 0.05 Pa.

McKee and Frank (1981) examined the corrosion behavior of several experimental alloys in a simulated helium environment (see their Table 7 for gas composition) to evaluate the role of alloying additions such as Al, Ti, Si, Nb, and Y in a base composition of Ni-20 wt.% Cr. Experiments were conducted for 1000 h at 750 and 850°C and for 1000 and 3000 h at 950°C. The alloys exhibited considerable variation in corrosion behavior over these test conditions. In general, carburization was more severe at 950°C than at lower temperatures. Alloys containing Al were susceptible to internal oxidation at all three temperatures and to carburization at 950°C. Additions of Nb promoted formation of protective oxide scales at all three temperatures. Alloys containing Si were resistant to carburization but the scales tended to spall. Alloy containing 1 wt.% Y exhibited massive precipitation of Cr carbides and poor corrosion performance at 950°C.

Cappellaere et al. (1984) examined the influence of helium pressure on the corrosion of ferritic and austenitic materials by conducting tests at 2 atm in a circuit without helium recirculation and at 50 atm in the AIDA loop. The gas chemistries in both these experiments were the same (Table 3.2). Experiments were conducted with HT 9 ferritic steel, Types 304 and 316 austenitic stainless steels, Alloys 800H and 617, and Hastelloy X. Specimens were exposed at temperatures between 550 and 870°C for time periods up to 10,000 h at 2 atm and for 2,500 h at 50 atm. Several conclusions were drawn from the study:

- Up to 650°C, HT 9 ferritic steel and Types 304 and 316 austenitic steels, and Alloy 800H showed excellent corrosion performance.

- At 750 and 870°C, Hastelloy X exhibited better resistance to oxidation than Alloys 800H and 617. For all three alloys, the oxidation rates decreased with time, but the rates were ≈3 times higher for Alloys 800H and 617 when compared with Hastelloy X.

- In general, the oxidation rates at 50 atm were higher than those at 2 atm. At 870°C, the materials were more damaged after 2,500-h exposure in 50-atm tests, compared with 10,000-h exposure in 2-atm tests. Figure 3.6 shows a comparative plot of the corrosion behavior for the three alloys from 2- and 50-atm tests.

Huchtemann (1989) reported that in a helium environment with low oxygen pressure (see Table 3.2 for gas chemistry used), the Alloy 617 surface underwent an enrichment of titanium and had no manganese chromium spinel. In addition, an enhanced decarburization and internal oxidation of aluminum occurred.

Figure 3.7 is a comparative plot of the environments used in different research programs listed in Table 3.2. The carbon activity in this plot is based on Eq. (4), whereas the pO_2 is based on Eq. (12). Consistent with observations reported in several studies, a tentative line can be drawn depicting the transition from the carburizing to oxidizing environment for high chromium alloys. Even among the oxidizing environments, the alloy may undergo decarburization, if the protective scaling process is kinetically slow. The results presented here clearly show that significant additional tests are needed in well-controlled environments to

establish the mode of interaction for materials and its dependence on alloy and gas chemistry, exposure time, and temperature.

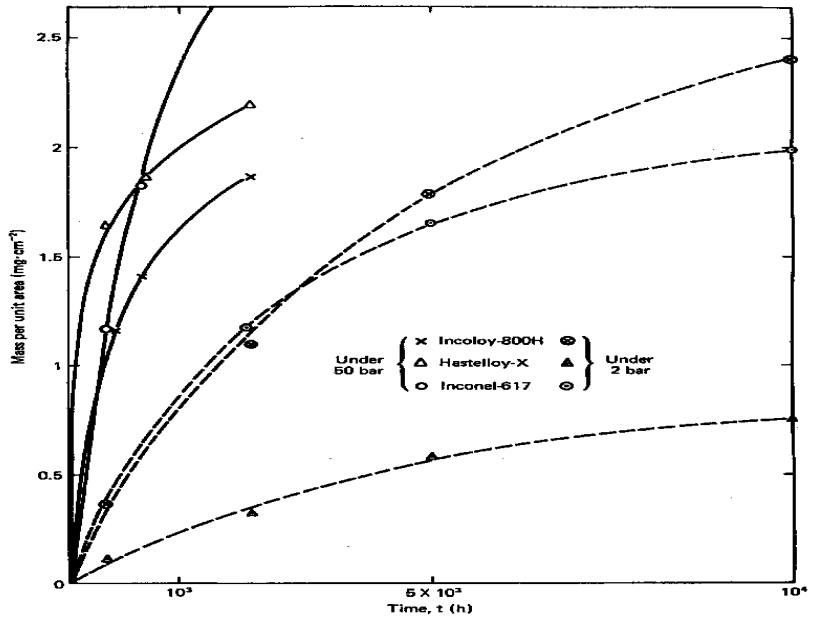

Figure 3.6 A comparative plot of corrosion behavior for Alloys 800H, Nimonic 86, and 617 from 2- and 50-atm tests (Cappellaere et al. 1984).

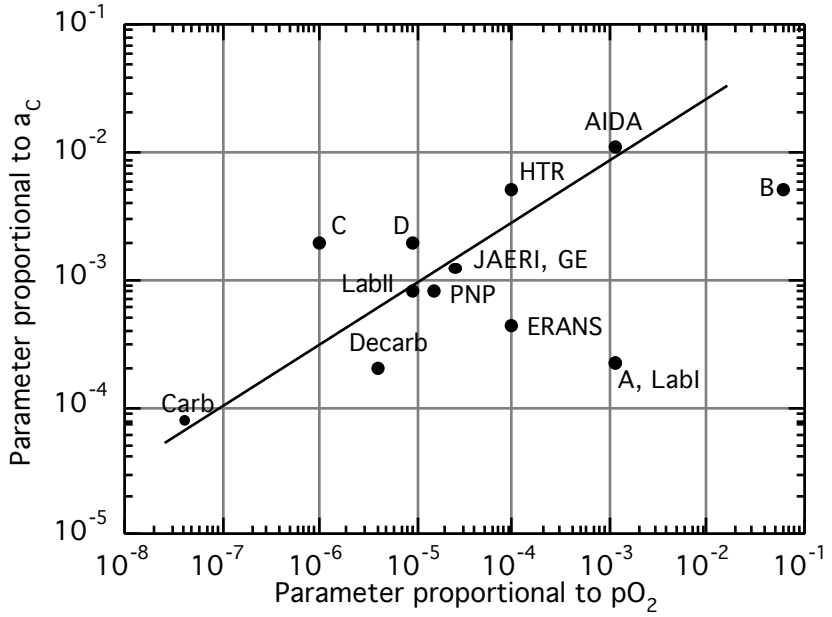

Figure 3.7 Comparative plot of the environments used in different research programs listed in Table 3.2. The carbon activity in this plot is based on Eq. (4), whereas the pO_2 is based on Eq. (12).

3.3 Effect of Impurities on Mechanical Properties

Several studies have been conducted to evaluate the mechanical properties of candidate alloys for structural applications and for power conversion systems. The mechanical properties evaluated in these studies include creep, creep rupture, low- and high-cycle fatigue, creep fatigue, and fracture toughness. Mechanical tests were conducted in a helium environment that contained impurities such as H_2, H_2O, CH_4, CO, and CO_2. The impurity levels were selected to simulate HTGR environments that contained sufficiently high H_2O (typical of steam-cycle-based HTGRs) so that the alloys predominantly developed oxide scales on the surface during mechanical testing.

3.3.1 Creep and Creep Rupture Properties

Several creep studies have been conducted on Alloys 800H, 617, Hastelloy X, Hastelloy XR, Nimonic 86, Manaurite 36X, and IN 519 in a "typical" reactor-helium chemistry that was estimated for steam cycle and process heat applications (Schubert 1984, Schubert et al. 1983, Schubert et al. 1984, Lee 1984, Kurata et al. 1984, Tanabe at al. 1984, Nakanishi and Kawakami 1984, Cook 1984, Ennis et al. 1984). Most of the studies have emphasized testing of Alloys 800H, 617, and Hastelloy X.

The mechanical properties, influence of the helium environment on the corrosion and mechanical performance, and design aspects of Alloy 800 are discussed in detail elsewhere (Betteridge, 1978) and are not elaborated further in this report. This report concluded that the influence of helium environment (with a chemistry typical of steam-based HTGRs) on the creep properties of the alloy is minimal at temperatures up to 760°C (see Figure 3.8), but that more work is needed to fully characterize the behavior at higher temperatures and longer times.

The creep curves of Alloy 617, especially at elevated temperatures of interest in HTGRs, show a monotonically increasing creep rate from the start of the test and virtually no secondary creep region (see Figure 3.9). This behavior is different from that of austenitic stainless steel, which distinctly shows primary, secondary, and tertiary creep regimes.

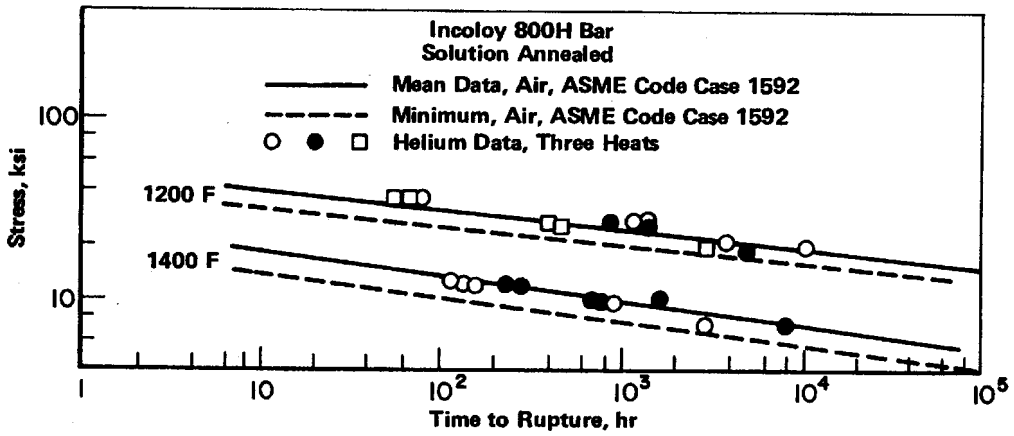

Figure 3.8 Creep rupture data for Alloy 800H at 650 and 760°C in helium with comparison to specifications based on air data in ASME Code (Roberts 1978).

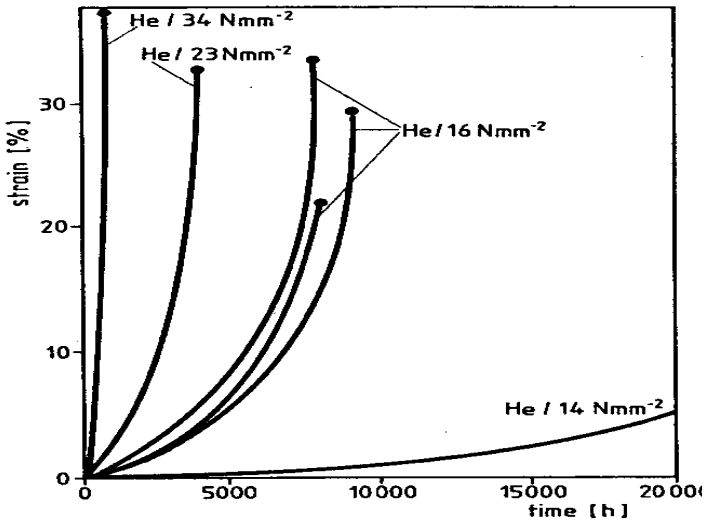

Figure 3.9 Creep curves for Alloy 617 at 950°C in a helium environment (Schubert et al. 1983).

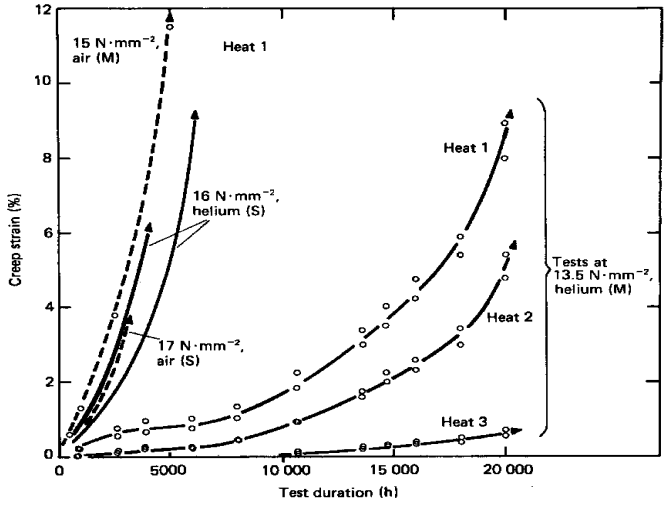

Figure 3.10 Heat-to-heat variation in the creep behavior of Alloy 617 in helium (Ennis et al. 1984).

Therefore, the creep data for Alloy 617 rarely include strain and time for onset-of-tertiary creep. At elevated temperatures, the creep properties of interest are the minimum stress for 1% creep strain and the rupture strength (Schubert 1983). In addition, the creep behavior of the alloy seems sensitive to factors other than composition, as evidenced by creep test data generated on three heats of the alloy (with nominally the same composition) in a helium environment (see Figure 3.10). As much as a factor of ten increase in rupture life was observed for a given applied stress for different heats of the alloy (Ennis et al. 1984).

Figure 3.11 shows the variation in creep rupture time with applied stress for Alloy 617 in air and helium at several temperatures, compiled by Ennis et al. (1984). The helium used in these experiments had a nominal composition (in Pa) of H_2:CO:CH_4:H_2O in the ratio of 50:5:5:0.15, except for those at 1000°C, in which the environment was decarburizing to the alloy. The few data points obtained at 1000°C under decarburizing conditions show a significant decrease in rupture life when compared with the data developed in air. Figure 3.12 shows data from another study conducted in helium that was decarburizing to Alloy 617 at 950°C (Huchtemann 1989). The impurity levels in helium in this experiment was (in Pa)

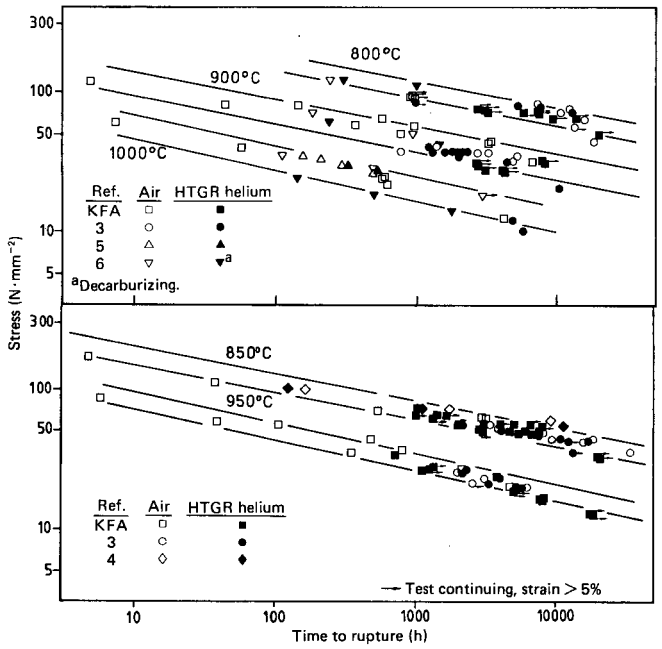

Figure 3.11 Variation in creep rupture time as a function of applied stress for Alloy 617 in air and helium at several temperatures (Ennis et al. 1984).

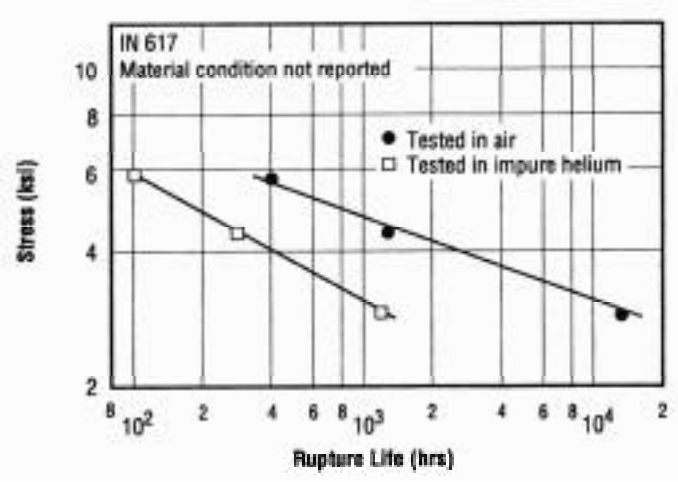

Figure 3.12 Variation in creep rupture time as a function of applied stress for Alloy 617 at 950°C in air and helium of low steam content (Huchtemann 1989).

H_2:CO:CH_4:H_2O:N_2 in the ratio of 50:1.5:2:0.015:0.5. The data show a significant decrease in creep life in helium when compared with that in air, for a given applied stress. Detailed examination of the tested creep specimens showed that Alloy 617 did not develop a protective oxide scale but exhibited significant internal oxidation of aluminum in the alloy accompanied by carbon loss. Note that the helium environment in the gas-turbine-based systems will be closer to the latter environment than those used in the study of either the steam-cycle system or the PNP.

Figure 3.13 shows the stress dependence of time to accumulate 1% strain and of time to rupture for Alloy 617 tested at 800 to 1000°C in air and in helium with "nominal" impurity levels (Schubert et al. 1983). The data, developed up to ≈20,000 h, indicate that the chemistry of the helium environment used had no significant effect on both the 1% strain and creep rupture properties, although the data set exhibits significant scatter.

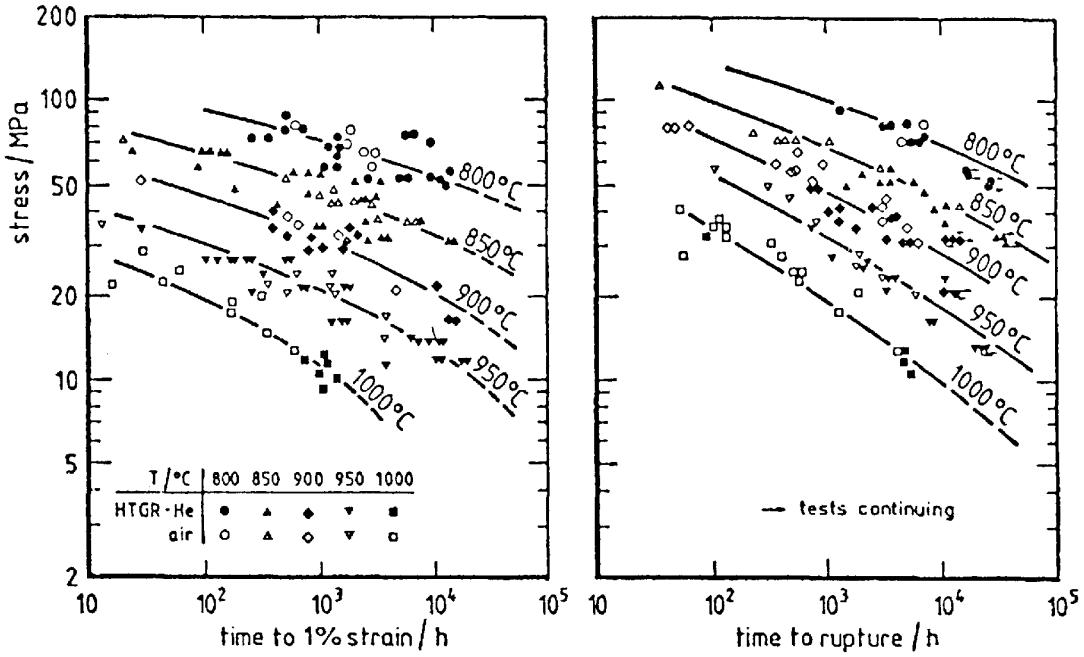

Figure 3.13 Time-to-1% strain and time-to-rupture as a function of applied stress for Alloy 617 in air and in HTGR helium (Schubert et al. 1983).

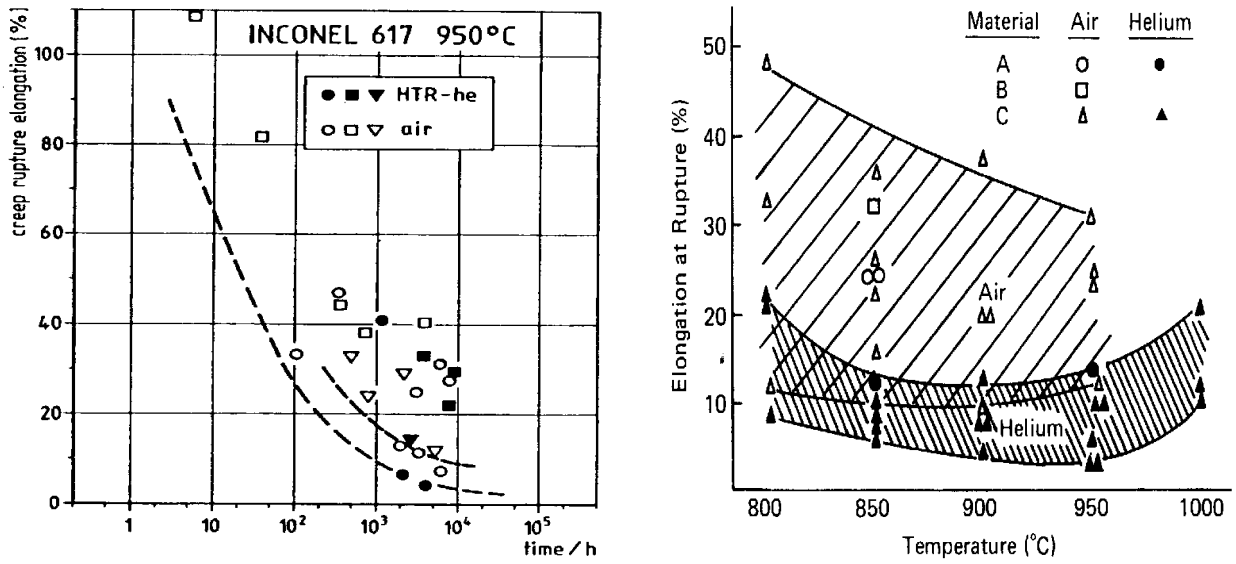

Figure 3.14 Creep rupture ductility of Alloy 617 in air and helium: (a) Schubert et al. 1983 and (b) Cook 1984.

One of the interesting creep properties to compare is the rupture ductility for Alloy 617 that has been tested in air and in helium. Figure 3.14 shows a plot of elongation at rupture from creep tests as a function of test time and temperature, obtained in two studies (Schubert et al. 1983, Cook 1984). The data indicate that the alloy had much lower ductility in helium compared to that obtained in air. Reason for these differences can be seen from the creep

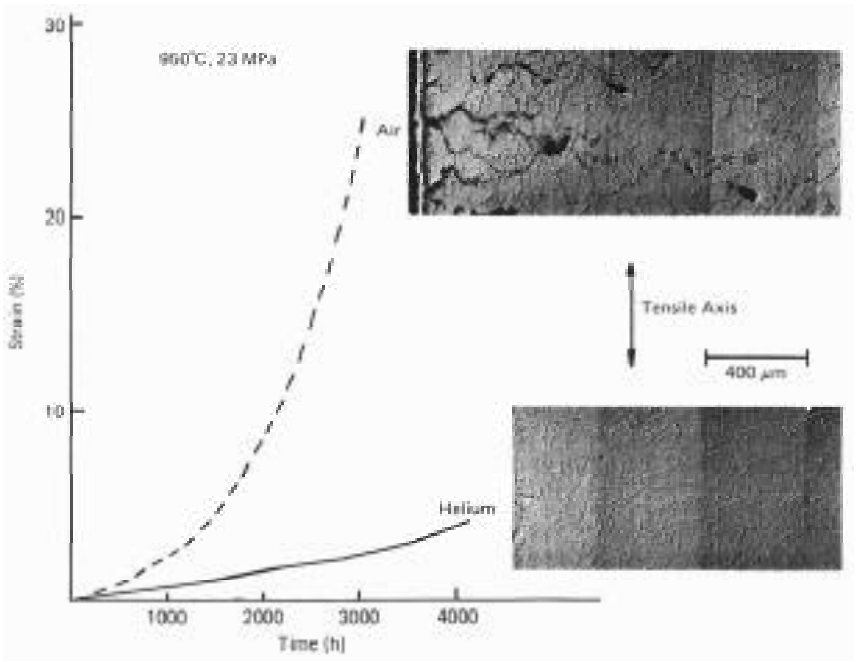

Figure 3.15 Examples of creep curves and cracking behavior for Alloy 617 tested in air and in helium at 950°C (Cook 1984).

curves and microstructures in Fig. 3.15, where air testing apparently induced surface cracks early in the test, leading to higher initial creep rates (Cook 1984). In helium, the shape of the creep curve indicated nucleation of surface cracks to be more difficult and virtual absence of "tertiary" creep. Rupture was reported without development of a large number of creep cracks in the helium environment. The apparent improvement of ductility in air was attributed to a combination of oxidation and crack growth.

3.3.2 Fatigue Properties

Several low- and high-cycle fatigue studies have been conducted on Alloys 800H, 617, Hastelloy X, and Hastelloy XR (Meurer et al. 1984, Soo and Sabatini 1984, Tsuji and Kondo 1984, Strizak et al. 1982, Kitagawa et al. 1979).

Strain-controlled fully reversed fatigue tests were conducted from room temperature to 871°C and at a cyclic strain rate of 4×10^{-3}/s (Strizak et al. 1982). The helium environment had a composition of (in Pa) H_2:CO:CH_4:H_2O in a ratio of 30:2:3:0.2. Figures 3.16 and 3.17 compare data generated for Alloy 617 specimens in the solution-annealed and solution-annealed-plus-aged conditions, in which the aging and test temperatures were identical. The results on thermal aging showed that aging for 10,000 h at these temperatures before testing reduced fatigue life, but aging for 20,000 h improved fatigue life slightly. These changes were attributed to microstructural changes that were noted in posttest examination of specimens. Results of testing Alloy 617 in impure helium indicated an improved cycle life when compared with the life obtained in pure helium. Strizak et al. (1982) also compared the data generated in impure helium with those generated in air and concluded that the helium environment was in no case detrimental to fatigue life for the alloy but was usually beneficial. Figure 3.18 shows a comparison of the low-cycle fatigue behavior of Alloy 617 in air and helium with the design curves (Schubert 1984).

Kitagawa et al. (1979) evaluated the low-cycle fatigue and creep fatigue behavior of Alloy 617 at 1000°C in air and in helium. Figure 3.19 shows the low-cycle fatigue behavior of the alloy in air and in 99.99% pure helium. Kitagawa et al. also tested some precarburized specimens, the results for which are also shown in Figure 3.19. They concluded that the fatigue properties in four-nine helium improved due to decarburization of the alloy, whereas the precarburized specimens exhibited somewhat lower fatigue properties when compared with data obtained in air. Figure 3.20 shows the fatigue lives of Alloy 617 under strain hold conditions tested at 1000°C in helium. The fatigue lives decreased with an increase in strain hold time.

Figure 3.21 compares experimental data on creep fatigue of Alloy 617 with the linear summation rule for the creep and fatigue damage. It is evident that the damage under creep-fatigue conditions is much more than predicted based on the linear rule. Additional data under different loading scenarios are needed to develop a predictive capability on creep-fatigue damage in the alloy, especially for helium purity levels typical of gas-turbine-based HTGRs.

Strizak et al. (1982) also developed low-cycle fatigue data on Hastelloy X in solution-annealed and solution-annealed-plus-aged conditions in air and in impure helium. The results were similar to those observed for the Alloy 617 (see Figure 3.22).

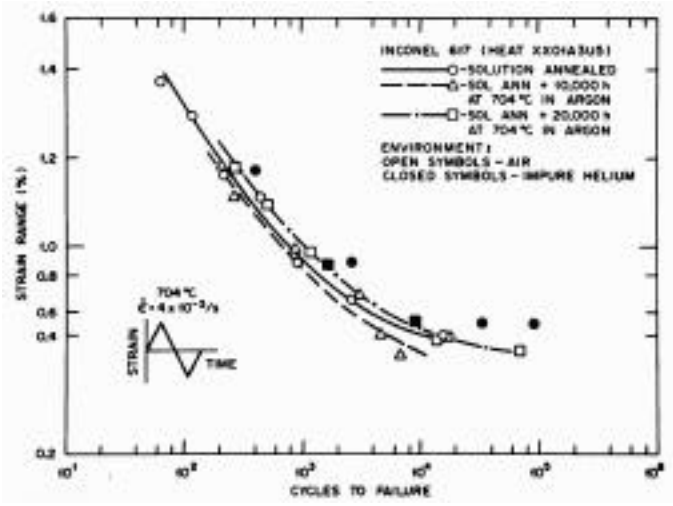

Figure 3.16 Comparison of low-cycle fatigue behavior of Inconel 617 tested in air and in helium at 704°C (Strizak et al. 1982).

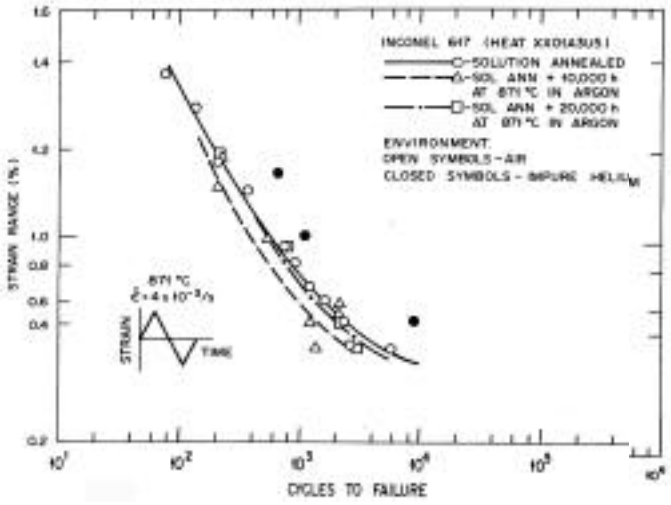

Figure 3.17 Comparison of low-cycle fatigue behavior of Inconel 617 tested in air and in helium at 871°C (Strizak et al. 1982).

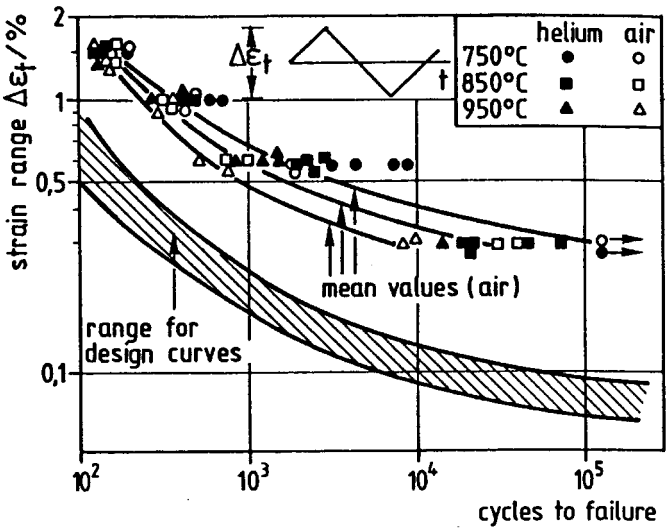

Figure 3.18 Comparison of the low-cycle fatigue behavior of Alloy 617 in air and in helium with the design curves (Schubert et al. 1983).

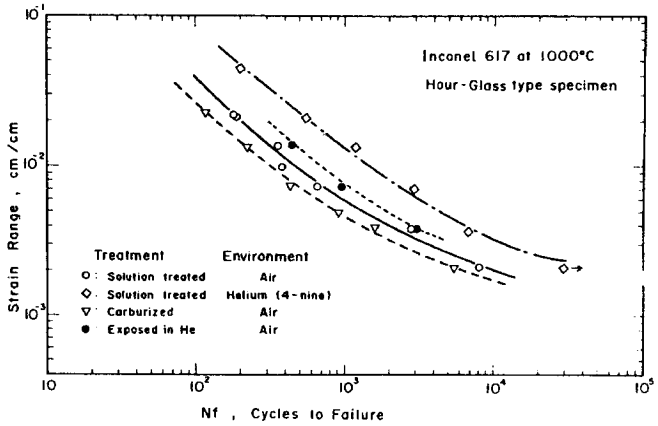

Figure 3.19 Comparison of low-cycle fatigue behavior of solution-treated and carburized Alloy 617 tested in air and in helium at 1000°C (Kitagawa et al. 1979).

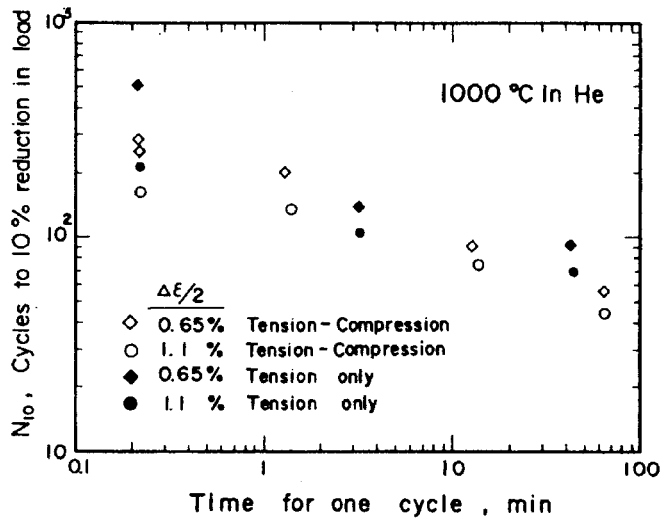

Figure 3.20 Influence of hold time on fatigue life of Alloy 617 at 1000°C (Kitagawa et al. 1979).

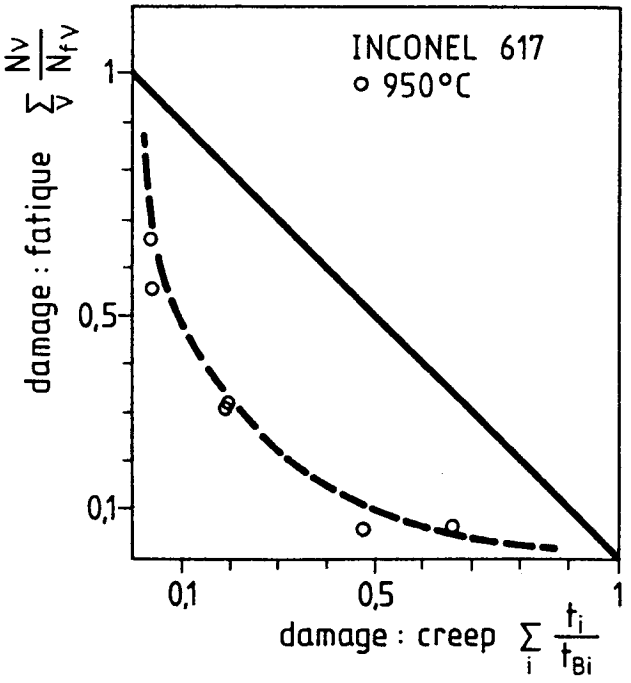

Figure 3.21 Comparison of experimental creep-fatigue data with linear damage accumulation rule (Schubert et al. 1983).

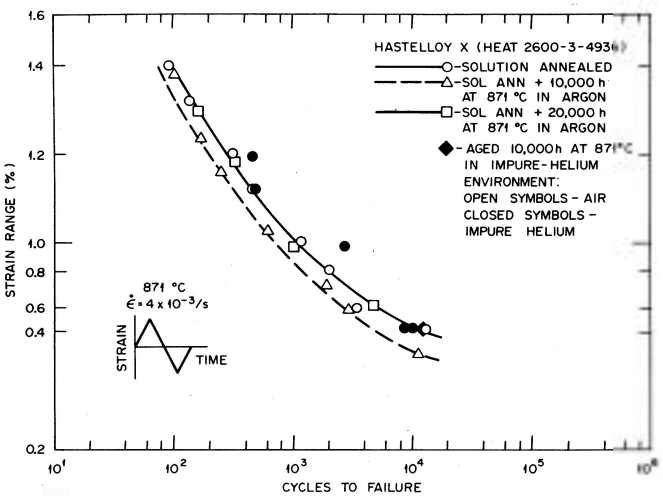

Figure 3.22 Comparison of strain-controlled fatigue data generated at 871°C in air and in helium for Hastelloy X in several conditions (Strizak et al. 1982).

3.3.3 Other Properties

Studies on creep and fatigue crack growth have been conducted with Nimonic 86 (Krompholz et al. 1984, Shahinian and Sadananda 1989).

Crack growth in nickel-base alloys IN-738 at 927°C under cyclic and static loads was investigated using fracture-mechanics-type specimens (Shahinian and Sadananda 1989). The influence of environment (specifically air, vacuum, and impure helium) on crack growth was examined. Crack growth was markedly slower on a time basis under static load (creep) than under cyclic load (fatigue), and in creep, crack growth required higher stress intensity for initiation. Generally, the resistance to crack growth in creep was faster in air than in vacuum, whereas in fatigue the converse was the case. The creep crack growth rates in helium containing small amounts of H_2, CO, and CH_4 were not significantly different from rates observed in vacuum.

4 Corrosion-Erosion

In systems that involve flow of particle-laden gases, one needs to consider corrosion-erosion as a mode of material degradation. Such information is needed to assess the long-term performance of candidate materials. Erosion, by itself, is a complex phenomenon and can be influenced by several variables, and combined erosion-corrosion is even more complex because of the dynamic changes that occur on the eroding surface due to gas-metal interactions.

The main operational experience with a gas stream that is laden with carbon-dust particles comes from the 15-MWe, Arbeitsgemeinshaft Versuchsreaktor (AVR), a pebble-bed-type HTGR. The reactor operated for ≈20 y and contained ≈100,000 fuel balls. At the end of 20-y operation, 60 kg of carbon dust was collected. This corresponds to ≈0.03 g/ball·y. Assuming the carbon dust particles are ≈1 μm dia, the number of particles created would be ≈2 x 10^9 particles/ball·y. If one assumes an average helium inventory in the reactor of 10 m^3, the particle density in the gas stream would be 2 x 10^{13} particles/m^3·y, or 4 x 10^{14} particles/m^3 at the end of 20-year operation or end of reactor life. In a closed-loop cycle, the helium replenishment is of the order of 0.1%/day, which means the entire helium inventory changes approximately every 3 years, and the dust loading increases with the aging of the reactor. The AVR experience shows that the blowers were significantly degraded over the years, and the cause was not reported. One of the causes for the dust in the AVR was attributed to an excessive release during control rod insertions into the reactor core. In the proposed current design with separate channels for coolant and control rod insertions, the dust loading may be less than that in AVR.

The PBMR-type reactor will contain on the order of 1.2 million fuel balls, and the helium inventory will be correspondingly high. However, the particle density will probably be less than that for the AVR since special channels, with no helium flow, are proposed for the control rod insertions. From the erosion standpoint, the consequences of particle flux, temperature, and particle size on the structural materials and on direct-driven gas-turbine materials are not known.

From the erosion-corrosion standpoint, degradation of materials is strongly influenced by factors such as erodent hardness, erodent size, temperature, substrate mechanical properties, and particle flux and velocity (Majumdar et al. 1988). An assessment of the erosion performance of structural alloys with different erodents showed that the erosion rate increases with the hardness of the erodent. Carbon dust particles with an average Vickers hardness of 20 and an average particle size of 1 μm (assuming no agglomeration) will tend to deposit on the surfaces of components rather than cause erosive wear.

The deposits on the surfaces of structural components and power conversion components alter the chemistry and thereby disrupt the protective capacity of the scales, if any, against corrosion. Liu and Natesan (1988) have examined methodologies for assessing and predicting metal oxidation-vaporization-erosion. The study examined the synergistic interaction of oxidation and erosion of metals and alloys by considering three competing processes: oxide scale thickening via growth, thinning via vaporization, and erosion. The authors demonstrated that not only do the models numerically reproduce the general features of oxidation-erosion observed in the few reported experiments on pure metals and alloys, but they also provide considerable insight into the conditions under which one mode (oxidation or erosion) can

become dominant over the other. Such a corrosion-erosion analysis of the reactor system and the power conversion system may be useful in evaluating and quantifying the issue and may also shed light on the purification scheme needed for the helium supply and replenishment and chemistry control.

5 Design Methodology

A companion report (Shah et al. 2003) reviews and evaluates currently available national and international codes and procedures for use in the design of HTGRs, including, but not limited to, the GT-MHR design and the PMBR. That report evaluates the applicability of the codes, standards, and procedures for the metallic materials that have been used or recommended for HTGRs, taking into account the HTGR operating temperature and environments. Seven codes and procedures [five ASME Codes and Code Cases, one French Code (RCC-MR), and one British Procedure] were reviewed and evaluated. The ASME Codes and Code Cases included Section III, Subsection NB and Subsection NH; Code Cases N-499-1, N-201-4; and the draft Code Case for Alloy 617. Two major findings were obtained. (1) The maximum temperature permitted by the codes and code cases for the materials acceptable for HTGR components, except for those made of Alloy 671, is lower (760°C) than the maximum temperature (850°C or higher) that these components may experience in reactor service. The scope of the code and code cases needs to be expanded to include materials with allowable temperatures of ≥850°C. (2) The codes and code cases do not provide specific guidelines for environmental effects, especially the effect of impure helium, on the high temperature behavior (e.g., creep and creep-fatigue) of the materials considered. The report concluded that needed data on environmental effects should be collected or generated, if not available, so that specific guidelines can be developed for these effects.

6 Off-normal Situations

Several off-normal situations can arise and lead to changes in the environment within the reactor and thereby can impact the metallic components, such as reactor internals, piping, power conversion systems, etc. These include

- Loss of coolant
- Air and/or steam ingress
- Particulate-laden gases

6.1 Loss of Coolant

The loss of coolant can increase the temperature of the reactor core, thereby causing failure of fuel pellets and release of fission products. Fission products such as Cs, Sr, and I can affect the structural materials, depending on how much is released and for how long the release was present during this off-normal event. However, a system such as GT-MHR has three main protective barriers to confine fission products (IAEA 2001). Figure 6.1 show a schematic for fission-product barriers and retention properties of TRISO fuel elements for a typical HTGR. The barriers include:

- The fuel kernel: The fuel is effective in confining solid fission products and partially retains gaseous and volatile fission products. The fuel temperature level and burnup are limited in design to enable confinement of fission products within the fuel kernel.
- Fuel kernel coatings: The next and most important barrier for fission product confinement is the protective coating on each fuel kernel. The GT-MHR design uses fuel with coatings made from three layers of pyrolitic carbon of different density and one layer of SiC. Experimental studies with coated particles of this type have validated their capability to confine fission products up to 1600°C, which corresponds to the maximum possible temperature level under emergency conditions.
- Graphite: The graphite of the fuel compacts and fuel blocks where the fuel particles are located can act as a barrier to confine fission products (such as Cs, Rb, Se, Ba, rare-earth elements) fairly effectively.

In addition, the fraction of particle failures during manufacture had a specification of $\leq 6 \times 10^{-5}$; that is, on average, one particle with a defective SiC layer is to be expected in two to three fuel spheres (Kroger et al. 1988). Also, TRISO coatings do not start to thermally degrade until temperatures approach 2000°C (LaBar 2002). Normal operating temperatures do not exceed about 1250°C. Even in the worst case, temperatures can be maintained below 1600°C (see Figure 6.2). Based on this analysis, a minimal release of fission products is expected, and its effect on the metallic structural materials is probably negligible.

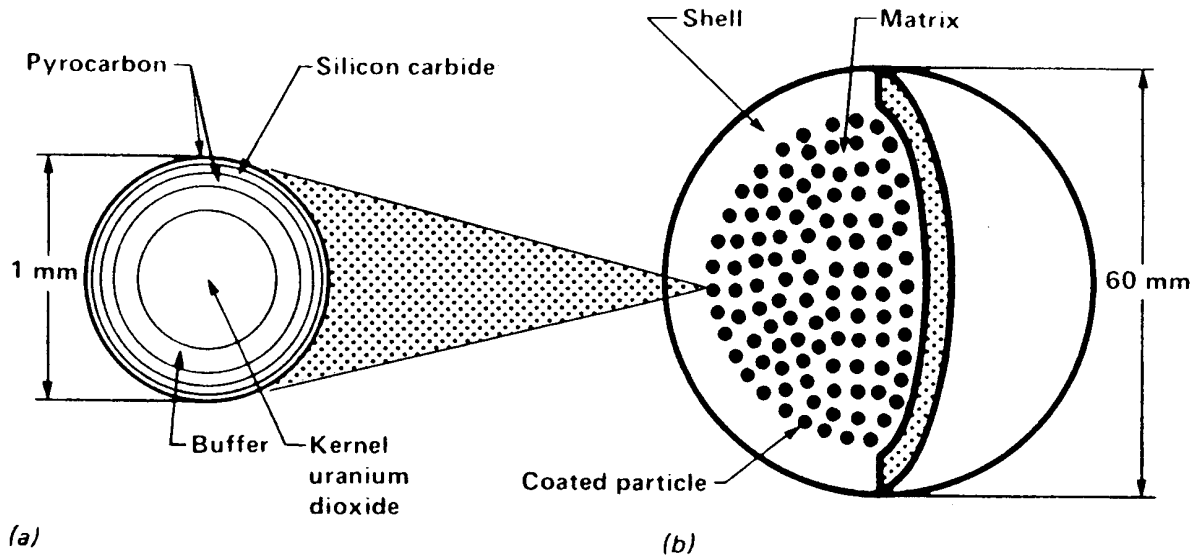

Figure 6.1 Fission-product barriers and retention properties of TRISO fuel elements for a pebble-bed gas reactor: (a) particle and (b) fuel element (Kroger et al. 1988).

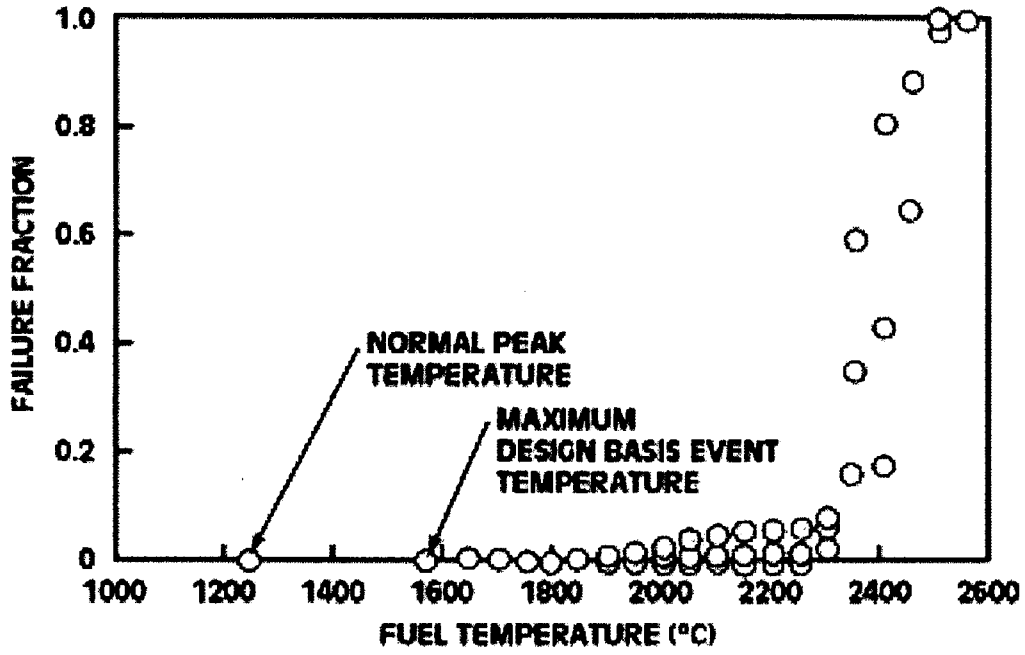

Figure 6.2 Coated-particle fuel temperature capability (La Bar 2002).

6.2 Air and Water Ingress

The potential ingress of air or steam can lead to a significant reaction with the graphite in the core and possibly with the fuel coatings. Such a reaction would significantly change the

chemistry of the helium coolant. In turn, this change can impact the reliability and integrity of metallic components. Katscher and Moormann (1986) have analyzed the kinetics of reactions between the structural graphite and the oxygen, carbon dioxide, and water vapor that are present due to accidental ingress. They calculated maximum burnoff rates for graphite with an unlimited supply of oxygen and concluded that there is uncertainty in the calculations influenced by the size and location of the leaks, ingress rate of air, mixing processes, etc.

The GT-MHR design includes technical measures that make the ingress of air or steam into the core less likely and also allow for decreasing the consequences should this event occur (IAEA 2001). These measures include:

- The working pressure of water in the PCS coolers and helium/water heat exchanger is considerably less than the helium working pressure in the primary circuit (≈7 MPa in this circuit versus 0.35 to 0.80 MPa in the intermediate water circuit in PCS coolers). This nearly eliminates the possibility of water ingress into the core during reactor power operation or cool down, if pressurized conditions are maintained in the primary circuit.

- Implementation of the "leak before break" concept limits the scope of a potential loss-of-integrity event in the vessel system. The leak-tight containment minimizes accidental ingress of air into the reactor. In the event of air leakage, helium is replaced by air over a long duration due to mass exchange and diffusion processes. The amount of air flow would be small through the place of leakage. Gases generated by the graphite oxidation process prevent the air coming to the core graphite structures, thereby moderating the oxidation process. The graphite temperature decreases during the reactor cool down to ≈600°C, which leads to shutting down of the oxidation process. It was estimated that not more than 1% of the total graphite mass would be subjected to corrosion. The impact of helium with such impurity levels, albeit for short times, on the metallic components is not established.

6.3 Particulate-Laden Gases

One of the purposes of the helium services system (HSS) in the GT-MHR is to maintain the primary coolant composition at specified levels to provide necessary conditions for long-term and reliable operation of the primary circuit components at normal operation and in accidents associated with water or air ingress into the primary circuit (IAEA 2001). The HSS includes the helium purification system (HPS), which consists of the equipment for helium cleanup of chemical and radioactive impurities, heat exchange equipment, pipelines, valves, instrumentation sensors, and the means for regeneration.

The HPS ensures the following levels of impurities in the helium under normal operating conditions: H_2O < 2 vppm, CO_2 + CO < 6 vppm, H_2 < 5 vppm. The primary helium flow rate through the HPS is 0.5 kg/s. The total helium flow rate through the core is 316 kg/s. This rate indicates that only about 0.15% of the reactor helium is replenished at any given time. Therefore, particulates such as carbon dust can accumulate in the helium stream as a function of time, even though the amount is not established. Furthermore, the role of the carbon dust, if any, on the deposition and/or erosion of metallic structural materials and PCS materials is not known.

Even though the release of fission products during normal operation is projected to be negligible, Kroger et al. (1988) reported that based on AVR studies, 73% of the released cesium

would be deposited on cooler metallic surfaces, 5% would be borne by graphite dust, and the rest would be retained by the reflector graphite. The role of such a deposition on the metallic surfaces in the degradation, if any, of metallic components is not established. It has been mentioned that release of the fission products deposited in the primary circuit outside the core is possible in certain accident situations. In the case of reactor depressurization, dust-borne activity deposited in corners of the streaming channel or on surfaces exposed to flow can be remobilized by an increased flow velocity. The impact of these scenarios on the materials/components integrity is not known.

7 Summary and Recommendations

The advanced HTGR concept, currently considered by the Member States of the IAEA's International Working Group on Gas Cooled Reactors, involves helium as the coolant and a closed-cycle gas turbine for power generation with a core outlet/gas turbine inlet temperature of 850°C and a net plant efficiency of 47%. In these designs, the helium from the core is used directly to drive the turbines or indirectly to heat the air or nitrogen, which drives the turbines. The system concepts include the GT-MHR developed by a consortium led by General Atomics in the U.S., the PBMR designed by ESKOM of South Africa and British Nuclear Fuels of U.K., and the HTTR of Japan.

This report has reviewed and evaluated the available information on performance and on long-term behavior of materials in environments that are typical of helium-cooled gas reactors. As a part of this evaluation, we have identified the materials that have been used in HTGRs, their functions, and the environmental conditions under which they have operated. We likewise identified the materials to be used in new HTGRs, the functions they will serve, and the anticipated environmental conditions under which they are expected to operate. We evaluated those HTGR conditions that may affect material property response, such as the steady-state operating environment, component geometry, and off-normal situations. Several conclusions were drawn from this evaluation:

- The majority of materials research and development programs in support of HTGRs was conducted in the 1960s to early 1980s. The thrust of these programs was to develop a database on materials for application in steam-cycle and process-nuclear-heat based HTGRs.

- Very little work was done on materials with emphasis on direct and/or indirect gas-turbine-based HTGRs during this period.

- The primary materials for high temperature application in HTGRs that have been evaluated in detail are Alloys 800H and 617 and Hastelloy X. Among them, Alloy 800H is code certified for temperatures up to 760°C for use in nuclear systems. A draft code case for Alloy 617 has been developed. A substantial database has been developed for both Alloys 800H and 617, and a limited database exists for Hastelloy X. Since the high temperature scaling in Hastelloy X has not been adequate, a modified version Hastelloy XR has been developed in programs conducted in Japan.

- Extensive analysis was made on the influence of helium coolant on the chemical compatibility of structural materials that are planned for use in HTGRs. Even though helium, by itself, is inert towards the materials, it is often contaminated by small amounts of gaseous impurities such as H_2, H_2O, CH_4, CO, CO_2, and O_2 from a variety of sources in the reactor circuit. The gas chemistry and the thermodynamic activity for carbon and oxygen in the gas phase are difficult to ascertain because of the nonequilibrium nature of the gas mixture. Furthermore, most studies on gas chemistry simulations were performed close to atmospheric pressure, whereas the system pressure in the reactor is ≈7 MPa.

- Structural alloys can be significantly corroded by the gaseous impurities in helium at elevated temperatures. Past studies have shown that the corrosion of heat-resistant materials such as austenitic stainless steels, Alloy 800H, and Alloy 617 may involve oxidation, carburization, and decarburization, depending on the exposure temperature, carbon activity in the gas phase, and the alloy composition. Furthermore, the corrosion process is "dynamic" in that it is dictated by the exposure time, gas chemistry variations, integrity of the corrosion product scales, and presence of particulates in the gas phase. A thermodynamic framework that includes evaluation of chemistry under nonequilibrium conditions is presented in this report. The available corrosion information for several candidate alloys exposed to helium environments is evaluated to address the scaling behavior and its relationship to gas chemistry.

- Available data are reviewed on the mechanical properties of candidate alloys in a helium environment with low levels of impurities. In most of these tests the environment contained sufficiently high H_2O (typical of steam-cycle-based HTGRs), and the alloys predominantly developed oxide scales on the surface during mechanical testing. The mechanical properties evaluated included creep, creep rupture, low- and high-cycle fatigue, creep fatigue, and fracture toughness. The analysis showed that the damage under creep-fatigue conditions is much more than prediction based on the linear rule. Additional data on creep-fatigue under different loading scenarios are needed to develop a predictive capability on creep fatigue damage in the alloy, especially in helium purity levels typical of gas-turbine-based HTGRs.

- In studies that were conducted in a helium environment with reduced levels of H_2O, Alloy 617 did not develop protective oxide scales, and the creep properties of the alloy showed a decrease in life when compared with data generated in air. The aluminum content in Alloy 617 led to internal oxidation rather than an external scale, especially in environments with low oxygen partial pressure. It is believed that the impurity levels in gas-turbine based systems will be predominantly decarburizing since oxygen potential is expected to be much lower than that in steam-cycle based systems.

- Before materials performance can be assessed, it is essential to establish an operational window in terms of impurity levels and particulate concentrations in helium that can be maintained and controlled with certainty. It was demonstrated that not only do the corrosion and erosion models numerically reproduce the general features of oxidation and/or erosion observed in the few reported experiments on pure metals and alloys, but they also provide considerable insight into the conditions under which one mode (oxidation or erosion) can become dominant over the other. Such a corrosion-erosion analysis of the reactor system and the power conversion system may be useful in evaluating and quantifying the issue and may also shed light on the purification scheme needed for the helium supply and replenishment and chemistry control.

- Over the last 20 years, alloy manufacturers have developed several alloys with improved resistance to oxidation and to carburization/decarburization at elevated temperatures. These materials include Alloy 230, 602CA, microalloyed cast HP alloys, and W-containing Ni-base superalloys. It is beneficial to examine the scaling and

corrosion performance of these alloys (in addition to Alloys 617, Hastelloy X, etc.) in helium with low oxygen partial pressures for their viability in the HTGRs.

- An extensive database is needed on candidate alloys for application in turbines (both blades and disks), especially for direct-cycle systems.

- The off-normal situations addressed in this report are limited to those that can lead to an increase in temperature and/or change in the chemistry of the environment, both of which can impact the metallic components used within the reactor.

- The current status of the materials database for the pressure vessels, piping and internals, and power conversion applications are summarized in Tables 7.1-7.3.

Table 7.1 Summary of available thermomechanical data for alloys considered for pressure vessel and other non-core, lower temperature components

Property \ Alloy	2-1/4Cr-1Mo	P9	P91	P92	E 911	HT9	316 SS
Tensile Strength	√	√	√	√	√	√	√
Creep	√	√	√	√	√	√	√
Fatigue	√	√	√	√	√	√	√
Creep Fatigue	√	√	√	√	√	√	√
Long-Term Aging: Effects on Microstructure	√	√	√	√	√	√	√
Environmental Effects	X	X	X	X	X	X	X
ASME Code Approved	Yes	Yes	Yes	Yes	?	Yes	Yes

√ = Data sufficient; X = Additional data needed, especially in He environment.

Table 7.2 Summary of available thermomechanical data for various alloys considered for piping and internals

Property \ Alloy Name	800H	Hastelloy X	Inconel 617	Hastelloy XR	Nimonic-86	Manaurite	Inconel 519
Tensile Strength	ASME code approved for T ≤760°C. Tensile data available T ≤900°C	Limited data available for T ≤ 1200°C	Limited data available for T ≤ 1200°C	Limited data available for 1200°C T ≤ 1200°C	Limited data available for T ≤ 1200°C	Limited data available for T ≤ 1200°C	Limited data available for T ≤ 1200°C
Creep	Limited data available for T ≤760°C	Limited data available for T ≤ 1100°C	Limited data available for T ≤ 1100°C	Limited data available for T ≤ 1100°C	Limited data available for T ≤ 1100°C	Limited data available for T ≤ 1100°C	Limited data available for T ≤ 1100°C
Fatigue	Limited data available for T ≤760°C	Limited data available for T ≤ 1100°C	Limited data available for T ≤ 1100°C	D Limited data available for T ≤ 1100°C	Limited data available for for T ≤ 1100°C	Limited data available for for T ≤ 1100°C	Limited data available for for T ≤ 1100°C
Creep Fatigue	Limited data available for T ≤760°C	Limited data available for T ≤ 760°C	Limited data available for T ≤ 760°C	Limited data available for T ≤ 760°C	Limited data available for T ≤ 760°C	Limited data available for T ≤ 760°C	Limited data available for T ≤ 760°C
Aging	Limited data available for T ≤1200°C	Limited data available for T ≤ 1200°C	Limited data available for T ≤ 1200°C	Limited data available for T ≤ 1200°C	Limited data available for T ≤ 1200°C	Limited data available for T ≤ 1200°C	Limited data available for T ≤ 1200°C
Environmental: Effects, especially in He with controlled impurity	Susceptible to metal dusting at 400°C ≤ T ≤ 800°C	Need to generate data for creep, fatigue and creep-fatigue	Need to generate data	Need to generate data	Need to generate data	Need to generate data	Need to generate data
Code Case Status	Approved N-201-4 T ≤ 760°C	Not approved	Draft ASME code case at T ≤982°C	Not approved	Not approved	Not approved	Not approved

Table 7.3 Summary of available thermomechanical data for various alloys for power conversion applications*

Alloy / Property	713LC	MAR-M 004	M21	738	Udimet 520	Mo-TZM	A286	706	718	Waspaloy	Udimet 720	MA6000
Tensile	T ≤900°C	T ≤1200°C	T ≤1200°C	T ≤1200°C	T ≤1200°C	T ≤1200°C	T ≤1200°C	T ≤1200°C	T ≤1200°C	T ≤1200°C	T ≤1200°C	T ≤1200°C
Creep	T ≤°C	T ≤1100°C	T ≤1100°C	√	√	√	√	√	√	√	√	√
Fatigue	T ≤°C	T ≤1100°C	T ≤1100°C	√	√	√	√	√	√	√	√	√
Creep Fatigue	X	X	X	√	√	√	√	√	√	√	√	√
Aging	X	X	X	√	√	√	√	√	√	√	√	√
Environmental effects	X	X	X	X	X	X	X	X	X	X	X	X
Code case status	NA	NA	NA	NA	NA	NA	NA	NA	NA	NA	NA	NA

√ = Limited data available; X = Need to generate data and develop phenomenological performance-based models; NA = Not approved.

*Power conversion requires high temperatures. Currently, no ASME code case covers the temperature range of interest (≈900-1100°C).

References

ASME, 1977, Boiler and Pressure Vessel Code Case 1592, Section VIII, American Society of Mechanical Engineers, New York.

Bassford, T. H. and T. V. Schill, 1979, "A Review of Inconel Alloy 617 and Its Properties after Long-Time Exposure to Intermediate Temperatures," Applications of Materials for Pressure Vessels and Piping, MPC-10, American Institute of Mechanical Engineers, San Francisco, CA, 1.

Bates, H. G. A., 1984, "The Corrosion Behavior of High-Temperature Alloys during Exposure for Times up to 10,000 h in Prototype Nuclear Process Helium at 700 to 900°C," Nuclear Technology, 66, 415.

Been, R. C., 1987, "Oxide Dispersion Strengthened Superalloys for Long-Term Service," Third Intl. Conf. on Creep and Fracture of Engineering Materials and Structures, Wales, U.K., 319.

Betteridge, W., et al. Eds., Proc. Conf. on Alloy 800, Petten, The Netherlands, March 14-16, 1978, North-Holland Publishing Company, Amsterdam, 1978.

Blackburn, L. D., 1972, "Isochronous Stress-Strain Curves for Austenitic Stainless Steels," The Generation of Isochronous Stress-Strain Curves, American Society of Mechanical Engineers, New York.

Blatherwick, A. A. and A. Cres, 1966, "Fatigue, Creep, and Stress-Rupture Properties of Nicrotung, Super A-286, and Inconel 718," Air Force Materials Laboratory, AFML TR65-447.

Booker, M. K., V. B. Baylor, and B. L. P. Booker, 1978, "Survey of Available Creep and Tensile Data for Alloy 800H," Oak Ridge National Laboratory, ORNL/TM-6029.

Boyer, V. S., et al., 1974. "Fulton Station HTGR," Nucl. Eng. Intl. August, pp. 635-659.

Brenner, K. G. E., 1982, in Proc. Conf. on Gas Cooled Reactors Today, British Nuclear Engineering Society, London, 191.

Brenner, K. G. E. and L. W. Graham, 1984, "The Development and Application of a Unified Corrosion Model for High-Temperature Gas-Cooled Reactor Systems," Nuclear Technology, 66, 404.

Brenner, K. G. E. and L. M. Nilsen, 1978, "High Temperature Materials Program Report 29," Central Institute for Industrial Research, Oslo, Norway.

Brey, H. L. 2000, "Developmental History of the Gas Turbine Modular High Temperature Reactor," IAEA-TECDOC--1238, presented at the IAEA Technical Committee Meeting on Gas Turbine Power Conversion for Modular HTGRs, held 14-16 November 2000, Palo Alto, CA.

Brinkman, C. R., D. J. Alexander, and P. J. Maziasz, 1990, "Modified 9Cr-lMo Steel for Advanced Steam Generator Applications," paper 90-JPCINE-8, presented at the Joint ASME/IEEE Power Generation Conference, Boston, MA, October 21-25, 1990.

Brooks, J. W. and P. J. Bridges, 1988, “Metallurgical Stability of Inconel 718,” Sixth International Symposium on Superalloys 1988, Champion, PA, September 18-22, 1988, TMS-AIME, Warrendale, PA, 33.

Bruch, U., D. Schuhmacher, P. Ennis, E. te Heesen, 1984, “Tensile and Impact Properties of Candidate Alloys for High-Temperature Gas-Cooled Reactor Applications,” Nuclear Technology, 66, 357.

Brush, D. R., 2001, “An Introduction to the 9Cr-1Mo-V Alloys,” Valve Magazine, 13, No. 1, 2.

Buckthorpe, D., et al. 2002, “Investigation of High Temperature Reactor (HTR) Materials,” presented at the 2nd Information Meeting on High Temperature Reactor Materials (HTR), NNC Limited.

Canonico, D., 1994, Proc. Second Int. Conf. Interaction of Steels with Hydrogen in Petroleum Industry Pressure Vessel and Pipeline Service, October 19-21, 1994, Vienna, Vol. 2, 607.

Cappellaere, M., M. Perrot, and J. Sannier, 1984, “Behavior of Metallic Materials between 550 and 870°C in High Temperature Gas-Cooled Reactor Helium Under Pressures of 2 and 50 Bar,” Nuclear Technology, 66, 465.

Chopra, O. K., and K. Natesan, 1977, “Thermodynamic Equilibria of Multicomponent Gas Mixtures,” High Temp. Sci., 9, 243.

Chow, J. G. Y., P. Soo, and L. Epel, 1978, “Creep and Fatigue Properties of Incoloy 800H in a High Temperature Gas Cooled Reactor (HTGR) Helium Environment,” Proc. of the Petten Int. Conf. on Alloy 800, March 14-16, 1978, eds. W. Betteridge et al., North Holland, 331.

Cleveland, J., et al., 1997. “The Role of the IAEA in Gas-Cooled Reactor Development and Application,” in Design and Development of Gas Cooled Reactors with Closed Cycle Gas Turbines, IAEA-TECDOC-899, Vienna, 257-270.

Cook, R. H., 1984, “Creep Properties of Inconel-617 in Air and Helium at 800 to 1000°C,” Nuclear Technology, 66, 283.

Couturier, R. and C. Escaravage, 2000, “High Temperature Alloys for the HTGR Gas Turbine: Required Properties and Development Needs,” IAEA Technical Committee Meeting on Gas Turbine Power Conversion Systems for Modular HTGRs, 14-16 November 2000, Palo Alto, CA, International Atomic Energy Agency, Vienna (Austria), Technical Working Group on Gas-Cooled Reactors, IAEA-TECDOC-1238, 161-173.

Ebi, G. and A. J. McEvily, 1984, “Effect of Processing on the High Temperature Low Cycle Fatigue Properties of Modified 9Cr-1Mo Ferritic Steel,” Fatigue Eng. Mater. Struct., 7, No. 4, 299.

Ennis, P. J. and A. Czyrska-Filemonowicz, 2002, “Recent Advances in Creep Resistant Steels for Power Plant Applications,” OMMI Internet Journal, Vol. 1, No. 1.

Ennis, P. J., K. P. Mohr, and H. Schuste, 1984, “Effect of Carburizing Service Environments on the Mechanical Properties of High-Temperature Alloys,” Nuclear Technology, 66, 363.

EPRI, 2002, “Evaluation of Materials Issues in the PBMR and GT-MHR,” draft document, October 17, 2002, Electric Power Research Institute, Palo Alto, CA.

Graham, L. W., 1985, “High Temperature Corrosion in Impure Helium Environments,” High Temp. Technol. 3, 3.

Graham, L. W., 1990, “Corrosion of metallic Materials in HTR-helium Environments,” J. Nuclear Materials, 171, 76.

Graham, L. W., K. G. E. Brenner, and K. Krompholz, 1981, “The Behavior of High Temperature Alloys during Exposure in Impure Helium,” IAEA Specialists Meeting on High Temperature Metallic Materials for Application in Gas-Cooled Reactors, Vienna, Austria, May 4-6 1981, Report IWGGCR-4, paper K1.

Hoffman, C., 1982, “The Effects of Mechanical Cycling on the Substructure of Modified 9Cr-1Mo Ferritic Steel,” in Ferritic Steels for High Temperature Applications, ed., A. K. Khare, American Society for Metals, Materials Park, OH, 221.

Howson, T. E., F. Cosandey, and J. K. Tien, 1980, “Creep Deformation and Rupture of Oxide Dispersion Strengthened Inconel MA 754 and MC 6000E,” Fourth Intl. Symp. on Superalloys, TMS-AIME, Champion, PA, 53.

Howson, T. E., D. A. Mervyn, and J. K. Tien, 1980, “Creep and Stress Rupture of a Mechanically Alloyed Oxide Dispersion and Precipitate Strengthened Nickel-Base Superalloy,” Met. Trans. 11A, No. 9, 1609.

Hsu, S. S., 1991, “The Effects of Fatigue, Hold Time, and Creep on Crack Growth in High Temperature Environments: Ni-Cr-Co Alloy,” Scripta Metallurgica et Materialia, 25, No. 5, 1143.

Huchtemann, B., 1989, “The Effect of Alloy Chemistry on Creep Behavior in a Helium Environment with Low Oxygen Partial Pressure,” Materials Science and Engineering, A121, 623.

Huddle, R. A. U., 1971, in Proc. Conf. on Effects of Environment on the Properties of Nuclear Materials, British Nuclear Energy Society, London, 203.

Huntington Alloys, Inc., 1978, “Inconel Alloy 718,” 10M 7-78 T-39.

IAEA 2001. “Chapter 4: Review of the Gas Turbine-Modular Helium Reactor (GT-MHR) Plant,” Current Status and Future Development of Modular High Temperature Gas Cooled Reactor Technology, International Atomic Energy Agency, IAEA-TECDOC-1198, pp. 69-113.

International Atomic Energy Agency, 1990. “Gas Cooled Reactor Design and Safety,” Technical Reports Series No. 312, IAEA, Vienna.

Jakobeit, W., 1983, “PM Mo-TZM Turbine Blades-Demands on Mechanical Properties,” R & HM.

Johnson, W. R. and G. Y. Lai, 1981,"Interaction of Metals with Primary Coolant Impurities: Comparison of Steam-Cycle and Advanced HTGRs," in Specialist Meeting on High Temperature Metallic Materials for Application in Gas Cooled Reactors, Paper J1.

Jones, W. B., 1983. "Effects of Mechanical Cycling on the Substructure of Modified 9Cr-1Mo Ferritic Steel," in Proc. ASM International Conference on Production, Fabrication, Propperties, and Application of Ferritic Steels for High-Temperature Applications, Wrren, PA, 6-8, October 1981, American Society for Metals, Metals Park, OH, 221-235.

Katscher, W. and R. Moormann, 1986, "Graphite Corrosion under Severe HTR Accident Conditions," IAEA Specialists' Meeting on Graphite Component Structural Design, JAERI, Japan, September 8-11, 1986, Paper III-9, 182.

Kitagawa, M., J. Hamanaka, T. Umeda, T. Goto, Y. Saiga, M. Ohnami, and T. Udoguchi, 1979, "A New Design for 1.5 MWt Helium Heat Exchanger," Trans. 5th Intl. Conf. on Structural Mechanics in Reactor Technology, Berlin, Germany, August 13-17, 1979, Paper F9/1.

Kohler, B., 1995, "GT-MHR Turbocompressor Design Report," Allied Signal report No. 41-14039.

Kondo, T., 1981, "Development and Testing of Alloys for Primary Circuit Structures of a VHTR," IAEA Specialists Meeting on High Temperature Metallic Materials for Application in Gas-Cooled Reactors, Vienna, Austria, May 4-6, 1981, Report IWGGCR-4, paper B1.

Kröger, W., H. Nickel, and R. Schulten, 1988, "Safety Characteristics of Modern High-Temperature Reactors," Nuclear Safety, 29, No. 1, 36.

Krompholz, K., E. Bodmann, G. K. H. Gnirss, and H. Huthmann, 1984, "Fracture Mechanics Investigations on High-Temperature Gas-Cooled Reactor Materials," Nuclear Technology, 66, 371.

Kurata, Y., Y. Ogawa, and T. Kondo, 1984, "Creep and Rupture Behavior of a Special Grade Hastelloy-X in Simulated HTGR Helium," Nuclear Technology, 66, 250.

LaBar, M. P., 2002. "The Gas Turbine – Modular Helium Reactor: A Promising Option for Near Term Deployment," General Atomics, GA-A23952.

Lee, K. S., 1984, "Creep Rupture Properties of Hastelloy-X and Incoloy-800H in a Simulated HTGR Helium Environment Containing High Levels of Moisture," Nuclear Technology, 66, 241.

Liu, Y. Y. and K. Natesan, 1988, "Methodologies for Prediction of Metal Oxidation-Vaporization-Erosion," Argonne National Laboratory Report, ANL/FE-88-2.

Majumdar, S., K. Natesan, and A. Sarajedini, 1988, "A Review of Solid Particle Erosion of Engineering Materials," Argonne National Laboratory Report, ANL/FE-88-1.

McKee, D. W. and R. G. Frank, 1981, “Corrosion Behavior of Experimental Alloys in Controlled Purity Helium,” IAEA Specialists Meeting on High Temperature Metallic Materials for Application in Gas-Cooled Reactors, Vienna, Austria, May 4-6, 1981, Report IWGGCR-4, Paper I1.

Menken, G. et al., 1982, “Review of Gas/Metal Interactions in HTR Helium up to 950°C,” in Proc. Conf. on Gas Cooled Reactors Today, British Nuclear Energy Society, London, 185.

Meurer, H., G. Gnirss, W. Mergler, G. Raule, H. Schuster, and G. Ullrich, 1984, “Investigations on the Fatigue Behavior of High-Temperature Alloys for High-Temperature Gas-Cooled Reactor Components,” Nuclear Technology, 66, 315.

Moore, R. A., et al., 1982. “HTGR Experience, Programs, and Future Applications,” Nuclear Engineering and Design, 72, 153-174.

Muto, Y., et al. 2000, “Selection of JAERI's HTGR-GT Concept,” IAEA-TECDOC--1238, presented at the IAEA Technical Committee Meeting on Gas Turbine Power Conversion for Modular HTGRs, held November 14-16, 2000, Palo Alto, CA.

Nakanishi, T. and H. Kawakami, 1984, “Creep Properties of Hastelloy-X in Impure Helium Environments,” Nuclear Technology, 66, 273.

Natesan, K., 1976, “High–Temperature Corrosion,” in Proc. Conf. on Prevention of Failures in Coal Conversion Systems, eds. T. R. Shives and W. A. Willard, U.S. Department of Commerce, National Bureau of Standards Special Technical Publication 468, 159.

Nickel, H., 1989. “Present Status of the High Temperature Reactor in the Federal Republic of Germany,” in Proceedings of the Workshop on Structural Design Criteria for HTR, Julich, 31 January–1 February, 1989, Jul-Conf-71, Breitbach, G., F. Schubert, and H. Nickel (Eds.), pp. 59-77.

OKBM, 1997, “Final Report on Turbocompressor Materials,” Task PCS 4-8, Prod. PCS 4-8-3, Revision 0, Experimental Designing Bureau of Machine Building, Russia.

Osthoff, W., H. Schuster, and P. Ennis, 1984, “Creep and Relaxation Behavior of Inconel-617,” Nuclear Technology, 66, 296.

Quadakkers, W. J. and H. Schuster, 1984, “Thermodynamic and Kinetic Aspects of the Corrosion of High-Temperature Alloys in High-Temperature Gas-Cooled Reactor Helium,” Nuclear Technology, 66, 383.

Quadakkers, W. J. and H. Schuster, 1985, “Corrosion of High Temperature Alloys in the Primary Circuit Helium of High Temperature Gas Cooled Reactors. - Part 1: Theoretical Background and Part II: Experimental Results,” Werkstoff und Korrosion, 6, 141 and 335.

Roberts, D. I., 1978, “Design Codes and Lifetime Prediction Aspects for Alloy 800 for Nuclear and Non-nuclear Applications, ” Proc. Intl. Conf. on Alloy 800, J. R. C. Petten Establishment, Petten, The Netherlands, North Holland, 403.

Ross, E. W. and C. T. Sims, 1987, “Nickel-Base Alloys,” in Superalloys II, eds. C. T. Sims, N. S. Stoloff, and W. C. Hagel, John Wiley & Sons, New York, 97.

Schneider, K., W. Hartnagel, P. Schepp, and B. Ilschner, 1984, “Creep Behavior of Materials for High-Temperature Reactor Application,” Nuclear Technology, 66, 289.

Schubert, F., H. J. Seehafer, and E. Bodmann, 1983, “Status of Design Code Work in Germany Concerning Materials and Structural Apects for the Heat exchanger Components of Advanced HTRs,” J. Engineering for Power, 105, 713.

Schubert, F., U. Bruch, R. Cook, H. Diehl, P. J. Ennis, W. Jakobeit, H. J. Penkalla, E. T. Heesen, and G. Ullrich, 1984, “Creep Rupture Behavior of Candidate Materials for Nuclear Process Heat Applications,” Nuclear Technology, 66, 227.

Schubert, F., 1984, “ Evaluation of Materials for Heat Exchanging Components in Advanced Helium-Cooled Reactors,” IAEA Specialists Meeting on Heat Exchanging Components of Gas-Cooled Reactors, Duesseldorf, Germany, IWGGCR-9, 309.

Shah, V. N., S. Majumdar, and K. Natesan, 2003, “Review and Assessment of Codes and Procedures in HTGR Components,” Argonne National Laboratory Report, to be published.

Shahinian, P. and K. Sadananda, 1989, “Creep and Fatigue Crack Growth Behavior of Some Cast Nickel-Base Alloys,” Materials Science and Engineering, A108, 131.

Shenoy, A. S., and W. S. Betts, 1988, “Design Requirements for High Temperature Metallic Component Materials in the US Modular HTGR,” in Proc. of a Specialists Meeting held in Cracow, June 20-23, 1988, pp. 34-42.

Shindo, M. and T. Kondo, 1982, “Studies on Improving Compatibility of Nickel-Base Alloys with a High-Temperature Helium-Cooled Reactor (VHTR) Environment,” in Proc. Conf. on Gas Cooled Reactors Today, British Nuclear Energy Society, London, 179.

Sikka, V. K, C. T. Ward, and K. C. Thomas, K. C, 1981, in Proc. of Conference on Ferritic Steels for High Temperature Applications, Warren, PA, October 6-18, 1981, American Society of Metals, 65.

Soo, P. and J. G. Y. Chow, 1976, “Correlation of High and Low-Cycle Fatigue Data for Incoloy 800H,” Brookhaven National Laboratory Report, BNL-NUREG-50574.

Soo, P. and J. G. Y. Chow, 1978, “Correlation of high and low-cycle fatigue data for Incoloy 800H,” Proc. of the Petten Intl. Conf. on Alloy 800, March 14-16, 1978, eds. W. Betteridge et al., North Holland, 169.

Soo, P. and R. L. Sabatini, 1984, “High-Cycle Behavior of Incoloy 800H in a Simulated HTGR Helium Environment Containing High Moisture Levels,” Nuclear Technology, 66, 324.

Staubli, M., W. Benedick, J. Orr, F. Deshayes, and Ch. Henry, 1998, in Materials for Advanced Power Engineering, eds., J. Lecomte-Beckers, F. Schubert, and P. J. Ennis, Forschungszentrum Julich, Energy Technology Series, Volume 5, Part I, 87.

Strizak, J. P., C. R. Brinkman, M. K. Booker, and P. L. Rittenhouse, 1982, “The Influence of Temperature, Environment, and Thermal Aging on the Continuous Cycle Fatigue Behavior of Hastelloy X and Inconel 617,” Oak Ridge National Laboratory, ORNL TM-8130.

Swindeman, R. W., Sikka, V. K., Maziasz, P. J., 1998, “Evaluation of T91 after 130,000 Hours in Service,” in Fatigue, Environmental Factors, and New Materials, PVP-Vol. 374, American Society of Mechanical Engineers, New York, 305-312.

Swindeman, R. W., P. J. Maziasz, and C. R. Brinkman, 2000, “Aging Effects on the Creep-Rupture of 9Cr-1Mo-V Steel,” Proc. Intl. Joint Power Generation Conf., Miami, FL, July 23-26, 2000, IJPGC2000-15050.

Tanabe, T., Y. Sakai, T. Shikama, M. Fujitsuka, H. Yoshida, and R. Watanabe, 1984, “Creep Rupture Properties of Superalloys Developed for Nuclear Steelmaking,” Nuclear Technology, 66, 260.

Tsuji, H. and T. Kondo, 1984, “Low-Cycle Fatigue of Heat-Resistant Alloys in High-Temperature Gas-Cooled Reactor Helium,” Nuclear Technology, 66, 347.

Wachter, O., P. J. Ennis, A. Czyrska-Filemonowicz, A. Zielinska-Lipiec, and H. Nickel, 1995, Report of the Research Center Julich, Jul-3074, ISSN 0944-2952.

Williams, P. M., et al., 1994. “MHTGR Development in the United States,” Progress in Nuclear Energy, 28 (3), 265-346.